

CHANCES, The Chilean Cluster Galaxy Evolution Survey: selection and initial characterization of clusters and superclusters[★]

Cristóbal Sifón¹, Alexis Finoguenov², Christopher P. Haines³, Yara Jaffé⁴, B. M. Amrutha³, Ricardo Demarco⁵, E. V. R. Lima⁶, Ciria Lima-Dias^{7,8}, Hugo Méndez-Hernández^{7,8}, Paola Merluzzi⁹, Antonela Monachesi⁷, Gabriel S. M. Teixeira¹⁰, Nicolas Tejos¹, Pablo Araya-Araya⁶, Maria Argudo-Fernández^{11,12}, Raúl Baier-Soto⁴, Lawrence E. Bilton^{13,4,1,14}, C. R. Bom¹⁰, Juan Pablo Calderón^{15,16,17}, Letizia P. Cassarà¹⁸, Johan Comparat¹⁹, H. M. Courtois²⁰, Giuseppe D’Ago²¹, Alexandra Dupuy²², Alexander Fritz²³, Rodrigo F. Haack^{16,17}, Fabio R. Herpich²⁴, E. Ibar¹³, Ulrike Kuchner²⁵, Amanda R. Lopes^{16,17}, Sebastian Lopez²⁶, Elismar Lösch⁶, Sean McGee²⁷, C. Mendes de Oliveira⁶, Lorenzo Morelli³, Alessia Moretti²⁸, Diego Palleró⁴, Franco Piraino-Cerda⁴, Emanuela Pompei²⁹, U. Rescigno³, Rory Smith⁴, Analía V. Smith Castelli^{16,17}, Laerte Sodré Jr⁶, and Elmo Tempel^{30,31}

(Affiliations can be found after the references)

November 22, 2024

ABSTRACT

CHANCES, the CHileAN Cluster galaxy Evolution Survey, will study the evolution of galaxies in and around ~ 150 massive galaxy clusters, from the local universe out to $z = 0.45$. CHANCES will use the new 4MOST Spectroscopic Survey Facility on the VISTA 4m telescope to obtain spectra for $\sim 500,000$ galaxies with magnitudes $r_{AB} < 20.5$, providing comprehensive spectroscopic coverage of each cluster out to $5r_{200}$. Its wide and deep scope will trace massive and dwarf galaxies from the surrounding filaments and groups to the cores of galaxy clusters, enabling the study of galaxy pre-processing and the role of the evolving environment on galaxy evolution. In this paper we present and characterize the sample of clusters and superclusters to be targeted by CHANCES. We used literature catalogues based on X-ray emission and Sunyaev-Zel’dovich effect to define the cluster sample in a homogeneous way, with attention to cluster mass and redshift, as well as the availability of ancillary data. We calibrated literature mass estimates from various surveys against each other and provide an initial mass estimate for each cluster, which we used to define the radial extent of the 4MOST coverage. We also present an initial assessment of the structure surrounding these clusters based on the redMaPPer red-sequence algorithm as a preview of some of the science CHANCES will enable.

Key words. galaxies: clusters: general – large-scale structure of the Universe

1. Introduction

Understanding what drives the evolution of galaxies and determines whether they end up as star-forming spirals or quiescent early-type galaxies remains a fundamental task within astrophysics. While most isolated galaxies remain as gas-rich star-forming spirals to the present day, the bulk of galaxies within massive clusters have lost their gas and have been transformed into quiescent early-type galaxies (Wilman et al. 2009). Both internal energetic mechanisms and external environmental processes are expected to play major roles in transforming galaxies. The former may include gravitational instabilities, supernovae, stellar winds, or feedback from the central supermassive black hole. The latter can include gravitational processes, such as tidal stripping by the cluster halo and galaxy-galaxy interactions (e.g., Natarajan et al. 2002; Gnedin 2003; Smith et al. 2016; Tollet et al. 2017; Smith et al. 2022), and hydrodynamical processes due to the hot intracluster medium (ICM), such as gas heating or ram pressure stripping (e.g., Gunn & Gott 1972; Treu et al. 2003; Ebeling et al. 2014; Brown et al. 2017; Quilis et al. 2017; Kulier et al. 2023). For a review of these various effects see Boselli et al. (2022), and for one focused on environment-related scenarios see Alberts & Noble (2022).

It is now well established that a significant fraction of this transformation takes place not inside the clusters themselves, but in the surrounding filamentary large-scale structure, reaching out to at least $5r_{200}$. This is evidenced by a reduced level of star formation and a lower fraction of star-forming galaxies at large cluster-centric radii ($2-5r_{200}$) relative to coeval field galaxy populations (Hou et al. 2014; Haines et al. 2015; Lopes et al. 2024; de Vos et al. 2024). This shortfall of star-forming galaxies at large cluster-centric radii has been interpreted as evidence for star-forming galaxies being at least partially quenched within galaxy groups (Zabludoff et al. 1996), prior to their arrival into the clusters. This interpretation is supported by recent studies identifying galaxy groups in the infall regions of clusters. For instance, the fraction of star-forming galaxies within these groups is lower than seen among other galaxies at the same cluster-centric distance (Bianconi et al. 2018; Lopes et al. 2024) and than galaxies in groups not associated with more massive clusters (e.g., Montaguth et al. 2024). This cumulative effect of processes outside of the cluster is known as pre-processing of galaxies (Fujita 2004) and is also a topic of increased investigation in hydrodynamical simulations (e.g., Bahé et al. 2013, 2019; Palleró et al. 2022; Sifón & Han 2024).

Beyond groups and clusters, intermediate-density environments of the cosmic web (filaments and sheets) may play an equally important role in galaxy evolution. The cosmic web dynamically impacts about half of all galaxies falling into clusters

[★] The code used for the analysis and figures in this paper is publicly available at <https://github.com/4MOST-CHANCES/cluster-catalogues>.

(Cautun et al. 2014; Kuchner et al. 2022) and can be made responsible for gas accretion, secondary infall and disk reformations, but also for gas stripping and shock heating that lead to a star formation suppression (Martínez et al. 2016; Donnan et al. 2022; Hasan et al. 2023). In response, our model of how galaxies quench is now changing to account for the physical processes and time spent in filaments, walls and groups. Indeed, galaxies in filament cores are redder, more massive, and tend to be elliptical with lower star formation rates and higher metallicities. We currently do not know whether or not these observations are solely a consequence of the relations with local density (e.g., morphology-density and star formation-density) or if the physical processes in cosmic filaments are responsible for the observations. This is a topic of ongoing study with varying findings and dependencies on galaxy stellar mass (O’Kane et al. 2024; Raj et al. 2024).

The cosmic evolution of star formation in and around clusters provides another key piece to constrain the timescales of galaxy transformation (Haines et al. 2013; Stroe et al. 2017; Kesbonye et al. 2023). Indeed, the relevance of pre-processing to the evolution of present-day cluster galaxies is a consequence of both the late assembly of massive clusters – they have accreted half their mass and galaxy populations since $z \sim 0.5$ – and the fact that a significant fraction of this accreted material is in the form of galaxy groups (McGee et al. 2009). Indeed, Haines et al. (2018) showed that massive clusters contain a wealth of X-ray galaxy groups at distances $\sim r_{200}$, whose accretion can explain half of the expected mass growth rate of clusters at late epochs.

CHANCES¹, the CHileAN Cluster galaxy Evolution Survey (Haines et al. 2023), is a 4MOST Community Survey (de Jong et al. 2019) designed to uncover the relationship between the evolution of galaxies and hierarchical structure formation as it happens, through deep and wide multi-object spectroscopy of galaxy clusters and their surroundings. During its five-year survey, CHANCES will target $\sim 500,000$ cluster galaxies out to $5r_{200}$. This is approximately the distance at which environmental effects acting on infalling galaxies are expected to be sufficiently strong to start removing their extended hot gas atmospheres and cutting off their gas supply (Bahé et al. 2013). It is also well beyond the maximum distance of $2\text{--}3 r_{200}$ to which ‘back-splash’ galaxies can reach (Mamon et al. 2004; Kuchner et al. 2022; Pizzardo et al. 2024). In fact, $5r_{200}$ corresponds roughly to the turn-around radius, i.e., that within which matter has detached from the Hubble-Lemaître flow and is bounded to collapse gravitationally (e.g., Bertschinger 1985; Rines & Diaferio 2006). In combination with other multi-wavelength surveys, CHANCES will capture all relevant environments in and around massive clusters, including filaments and groups, to determine the prevalence of pre-processing, providing a comprehensive view of the evolution of galaxies and the growth of massive clusters over the past 5 Gyr. A complementary survey, the WEAVE Wide-Field Cluster Survey, will be performed in the northern hemisphere with the WEAVE multi-fiber spectrograph on the William Herschel Telescope, characterizing environmentally-driven galaxy evolution with breadth and depth comparable to CHANCES (Jin et al. 2024).

In this paper we present the cluster selection for CHANCES (Section 2). We then discuss a uniform calibration of cluster masses based on literature estimates used to define the radial extent of 4MOST coverage (Section 3). We also provide an initial evaluation of the infalling structures surrounding these clusters using a photometric cluster catalogue (Section 4). We conclude

with a summary and final remarks (Section 5). The CHANCES target selection and observational setup will be described in more detail in Haines et al. (in prep.) and other forthcoming papers.

Throughout this paper, M_{200} refers to the mass within r_{200} , corresponding to the radius enclosing a density 200 times the critical matter density of the Universe at each redshift. We assume a flat Λ CDM cosmology with cosmological parameters corresponding to the central values inferred by Planck Collaboration (2020), of which the most relevant are the current expansion rate, $H_0 = 67.4 \text{ km s}^{-1} \text{ Mpc}^{-1}$, and the present-day matter density parameter, $\Omega_m = 0.315$.

2. Survey design

The 4MOST Spectroscopic Survey Facility is a multi-fiber spectrograph about to be installed on the VISTA 4m telescope at Paranal Observatory in Chile. It is equipped with 2436 science fibers, 1624 of them feeding two low-resolution spectrographs with $R \equiv \lambda/\Delta\lambda = 6,500$ and 812 feeding a single high-resolution spectrograph with $R = 20,000$, which can be positioned across a 2.5-degree diameter field of view (de Jong et al. 2016, 2022). 4MOST will simultaneously carry out 18 public spectroscopic surveys over its first five years of science operations, sharing the focal plane among the surveys in every observation to maximize efficiency (de Jong et al. 2019; Tempel et al. 2020a,b).

With the 4MOST survey structure, we devised a strategy to study the evolution of galaxies in and around clusters combining unique breadth and depth. In order to efficiently span both stellar mass and lookback times, we split the CHANCES cluster survey into a Low- z subsurvey including clusters and superclusters at $z < 0.07$ and down to $M_{200} \sim 10^{14} M_\odot$ (Section 2.1), and an Evolution subsurvey consisting of massive ($M_{200} > 5 \times 10^{14} M_\odot$) clusters over $0.07 < z < 0.45$ (Section 2.2). We refer to these two collectively as the CHANCES cluster surveys; combined, they make CHANCES a survey with continuous coverage of massive clusters from the present day to $z = 0.45$, i.e., the past 4.8 Gyr of cosmic time. CHANCES is completed by a survey of the circumgalactic medium of cluster galaxies (CHANCES-CGM), which we briefly describe in Section 2.3 for completeness. Due to the 4MOST observing strategy we restrict CHANCES targets to declinations $-80^\circ < \delta < +5^\circ$. We also exclude clusters close to the Galactic plane.

By covering clusters out to $5r_{200}$ CHANCES will observe, in addition to the nominal cluster list, roughly ten times as many infalling systems with masses reaching about an order of magnitude lower than the main system (see Section 4.1). Thus CHANCES will provide an unprecedented view of environment-driven galaxy evolution, not only as a function of stellar mass but also of the masses of the main cluster and infalling groups. At a given cluster mass, we will also control for cluster large-scale environment, by assessing the impact of residing in a main cluster or in (or near) and infalling system such as a group or filament.

The primary requirement for a cluster to be included in CHANCES is the availability of photometry from the Dark Energy Camera Legacy Survey (DECaLS, Dey et al. 2019) data release 10 (LSDR10, Zenteno et al. in prep.), which ensures accurate astrometry and photometry over our entire survey. We make one exception with the Antlia cluster (Abell S636, $z = 0.0087$, i.e., part of the Low- z subsurvey; Lima-Dias et al. in prep.), which is not within the LSDR10 coverage, as it is an extremely nearby system with full coverage from the S-PLUS survey, which provides photometry in 12 narrow bands across the optical wavelength range (Mendes de Oliveira et al. 2019). Tar-

¹ <https://chances.uda.cl/>

get selection in the Antlia field relies on photometric redshifts based on S-PLUS photometry (Lima et al. 2022).

For both the Low- z and Evolution subsurveys we will target galaxies down to an r -band magnitude of 20.5, translating into stellar mass limits of $m_\star > 10^{8.5} M_\odot$ and $m_\star > 10^{10} M_\odot$, respectively. Selection of target galaxies is based on photometric redshifts from LSDR10 and, for a subsample of the Low- z subsurvey where S-PLUS data are available, from S-PLUS photometric redshifts, with stellar masses derived from the same photometry. Of the 500,000 spectroscopic targets within the CHANCES cluster survey, approximately 70% of the CHANCES targets will be devoted to the Low- z subsurvey, with 70% of those galaxies targeting individual clusters and the remaining 30% targeting the superclusters. Therefore we will target approximately 4500 galaxies per cluster in the Low- z cluster sample and approximately 2500 galaxies per Evolution cluster. Details will be presented in Haines et al. in prep. and Méndez-Hernández et al. in prep.

Figure 1 shows the CHANCES footprint on the sky: over 1,600 sq. deg. in all.² For visibility purposes we set each circle to have at least a 1 deg radius; in practice this means essentially all of the Evolution clusters are enlarged to this size, while all Low- z cluster footprints retain their original extents of $5r_{200}$. We describe the r_{200} estimates in Section 3. We also show several multi-wavelength surveys of interest: the Simons Observatory Large-Aperture Telescope (SO-LAT) survey (Simons Observatory Collaboration 2019, $-60^\circ \lesssim \delta \lesssim +20^\circ$), the Cerro Chajnantor Atacama Telescope (CCAT) Wide-Field Survey (WFS, CCAT-prime Collaboration 2023, $-61^\circ \lesssim \delta \lesssim +18^\circ$), and the Vera Rubin Observatory’s Legacy Survey of Space and Time (LSST, Ivezić et al. 2019, $-60^\circ \lesssim \delta \lesssim +2^\circ$), as well as the German half of the eROSITA all-sky survey, covering Galactic longitudes $l > 180^\circ$ (Merloni et al. 2024). Therefore in addition to its main science goals, CHANCES will also enable unique cluster and galaxy science in synergy with a rich array of multiwavelength data.

2.1. CHANCES Low- z subsurvey

The CHANCES Low- z subsurvey is designed to target 50 clusters at $z \leq 0.07$, in addition to covering large regions within the Shapley and Horologium-Reticulum superclusters, each containing a large number of clusters within a rich cosmic web.

2.1.1. Galaxy cluster sample

The Low- z subsurvey includes clusters selected from the All-Sky X-ray Extended Source (AXES) catalogue (Damsted et al. 2024; Khalil et al. 2024), the Wide-field Nearby Galaxy cluster Survey (WINGS, Fasano et al. 2006), and a number of clusters selected individually based on their known properties or available datasets. We describe each subset below.

AXES is a reanalysis of the ROSAT All-Sky Survey (RASS) data, in which X-ray emission from extended sources is detected on scales of 12–24 arcmin via wavelet decomposition (Damsted et al. 2024), which in the extragalactic area is complete down to a flux of 1×10^{-12} ergs $s^{-1} cm^{-2}$. AXES sources were initially validated against a group catalogue based on Sloan Digital Sky Survey (SDSS) data (Tempel et al. 2017) in Damsted et al. (2024), against the 2MRS galaxy group catalogue (Tem-

² This refers only to the cluster subsurveys described in Sections 2.1 and 2.2, i.e., excluding the CHANCES-CGM subsurvey briefly described in Section 2.3.

pel et al. 2018) in Khalil et al. (2024), and against a cluster catalogue constructed with the redMaPPer cluster red sequence finder applied to LSDR10 in Finoguenov et al. (in prep). We refer to these latter cross-matched catalogues as AXES-2MRS and AXES-LEGACY, respectively. The scales probed by AXES correspond roughly to $r_{500} - r_{200}$, which offers the unique advantage of using the scales where cluster behaviour is best understood. However, beyond $z = 0.04$ these angular scales extend beyond r_{200} and AXES sources become affected by blending. In addition, the feedback processes on low-mass clusters lead to baryonic lifting, resulting in additional flux compared to estimates based on L_{500} . This means the scales used in the AXES analyses are best suited to cluster characterization at $z < 0.04$ (Khalil et al. 2024; Damsted et al. 2024). Conversely, below $z = 0.01$ the scales used by AXES only probe cluster cores, changing the selection function.³ In any case, there are few massive clusters at such low redshifts, most of them with good auxiliary information. Therefore we use AXES-2MRS as our parent sample at $z < 0.04$.

WINGS, the Wide Nearby Galaxy cluster Survey (Fasano et al. 2006), together with its extension OmegaWINGS (Gullieuszik et al. 2015), is a multi-wavelength imaging and spectroscopic survey of 77 galaxy clusters at $0.04 \leq z \leq 0.07$ (perfectly complementing the redshift coverage of AXES-2MRS) that were selected from cluster catalogues constructed from the RASS. We include WINGS as one of the CHANCES Low- z parent catalogues because of the wealth of optical spectroscopy already available in the central regions of these clusters (Cava et al. 2009; Moretti et al. 2014, 2017). The 4MOST observations will complement the available data to reach the CHANCES specifications.

With these two parent samples, we design the Low- z subsurvey to cover an order of magnitude in mass at redshifts $z < 0.07$, sampling known clusters with an essentially uniform distribution in mass at $M_{200} \gtrsim 10^{14} M_\odot$, plus a few well-known lower-mass systems. The Low- z cluster sample is listed in Table A.1.

2.1.2. Superclusters

The CHANCES Low- z subsurvey also includes wide regions around two well-known superclusters: the Shapley supercluster at $z = 0.048$ (e.g., Reisenegger et al. 2000; Proust et al. 2006; Merluzzi et al. 2015; Haines et al. 2018) and the Horologium-Reticulum supercluster at $z = 0.060$ (e.g., Lucey et al. 1983; Fleener et al. 2005, 2006). The exact regions have been chosen as a compromise between the number of member clusters included and the available fibre hours for the entire survey. Spectroscopic targets will be selected homogeneously across the entire supercluster regions, ensuring a complete census of structure within them (Haines et al. in prep.).

The CHANCES coverage of the Shapley supercluster consists of 128 deg² plus the remaining area within $5r_{200}$ of Abell 3571. The coverage of the Horologium-Reticulum supercluster consists of 225 deg² plus the marginally overlapping $5r_{200}$ area around Abell 3266 (roughly half). Several other Low- z clusters overlap the superclusters in the sky (namely, Abell 3565 and Abell 3574 with Shapley and Fornax with Horologium-Reticulum). These clusters are at noticeably different redshifts than the superclusters so target overlap is limited to faint galaxies with large photometric redshift uncertainties (Méndez-Hernández et al. in prep.). This overlap will,

³ The lowest-redshift cluster in AXES-2MRS has $z = 0.0015$ and $M_{200} = 1.1 \times 10^{13} M_\odot$.

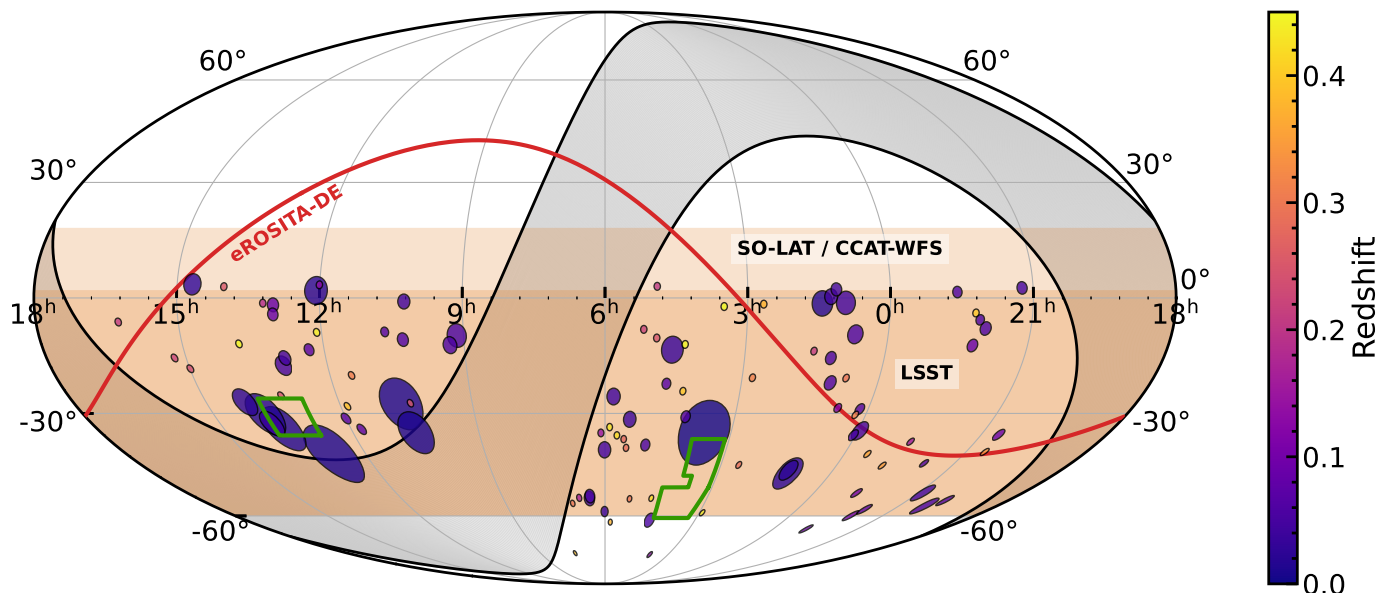


Fig. 1. Sky distribution of CHANCES clusters in Equatorial coordinates in a Mollweide projection. Each circle has a radius corresponding to the maximum between $5r_{200}$ and 1 deg (the latter set for visibility) and is colour-coded by redshift. The supercluster regions are shown with green polygons. The region below the red curve corresponds to the eROSITA-DE survey, the dark orange region shows the approximate LSST survey area, and the light orange region similarly for SO-LAT and CCAT-WFS (for simplicity we draw both as delimited by $-60^\circ \leq \delta \leq +18^\circ$). The grey band bounded by black lines shows Galactic latitudes $|b| \leq 20^\circ$.

in any case, ensure a high completeness for both the clusters and superclusters. The supercluster survey regions are shown in [Figure 1](#). The Shapley supercluster survey corresponds to a rectangle bounded by right ascensions $192^\circ \leq \alpha \leq 207^\circ$ and declinations $-36^\circ \leq \delta \leq -26^\circ$. The Horologium-Reticulum survey region is enclosed by the following polygon vertices⁴: [46.5, -51]; [49, -60.7]; [66, -60.7]; [66, -51]; [55, -51]; [55, -47.5]; [58.5, -47.5]; [58.5, -37]; [46.5, -37].

2.2. CHANCES Evolution subsurvey

As part of the CHANCES Evolution subsurvey we will target 50 of the most massive galaxy clusters distributed evenly over $0.07 < z < 0.45$. The Evolution sample is primarily selected from the second Planck catalogue of Sunyaev–Zel’dovich (SZ) sources (PSZ2; [Planck Collaboration 2016](#)), which provides a homogeneous sample of massive clusters over this redshift range. We select the ten most massive PSZ2 clusters with available DESI Legacy Imaging Survey DR10 grz imaging and photometric redshifts out to $5r_{200}$, in each of five linearly-spaced intervals over $0.07 < z < 0.45$. This binned selection ensures continuity with the Low- z subsurvey: there are eight Evolution clusters at $0.07 < z < 0.10$. It also translates to a minimum mass $M_{200} = 7 \times 10^{14} M_\odot$ at $z > 0.2$, while at lower redshifts the mass limit is progressively reduced to account for the smaller volume available. Most of the CHANCES Evolution cluster sample is covered by the CHEX-MATE XMM Heritage programme ([CHEX-MATE Collaboration 2021](#)), providing high-quality X-ray data suitable for characterising the ICM and mass distributions of each CHANCES cluster.

The only cluster in the Evolution subsurvey which is not matched to any PSZ2 source is MACS J0329.7–0211 at $z = 0.45$. We include it in CHANCES to take advantage of the extensive available spectroscopy thanks to the CLASH-VLT sur-

vey ([Rosati et al. 2014](#)). The Evolution cluster sample is listed in [Table A.2](#).

2.3. CHANCES CGM subsurvey

In addition to the cluster samples described above, CHANCES will offer a unique view of the circumgalactic medium (CGM) by observing $\sim 50,000$ galaxies around $\sim 10,000$ background quasars. Quasars are selected either from optical spectroscopy ([Lyke et al. 2020](#); [Anand et al. 2021](#)), or from X-ray imaging ([Merloni et al. 2019](#)), requiring that they lie within 6 Mpc in projection from foreground clusters at $0.35 < z < 0.7$, where the Mg II line falls in the wavelength range covered by 4MOST. Such experimental setup builds up from the one pioneered by [Lopez et al. \(2008\)](#). Clusters for the CGM subsurvey are selected from a catalogue constructed by applying the redMaPPer algorithm ([Rykoff et al. 2014](#)) to the LSDB10 data ([Kluge et al. 2024](#); see [Section 4](#)). The main goal of the CGM subsurvey is to establish the origin of intervening Mg II absorbers and their relation to galaxies as a function of galaxy type and both local and large-scale environment. In this manner, we will construct a detailed view of the CGM transformations occurring in dense environments and their impact on galaxy evolution, providing a novel complement to the CHANCES cluster survey. More details will be given in a forthcoming paper.

3. Cluster mass estimates

As described in the previous section, we have selected clusters homogeneously based on mass proxies from X-rays (Low- z) and the tSZ effect (Evolution). However, we use masses from a variety of sources in an attempt to obtain the best r_{200} estimate for each cluster while still maintaining some homogeneity in the mass estimates. To this end we cross-matched our cluster samples with several catalogues providing masses with different techniques, as summarized in [Tables 1](#) and [2](#). Given that we

⁴ These are given as $[\alpha, \delta]$ in degrees.

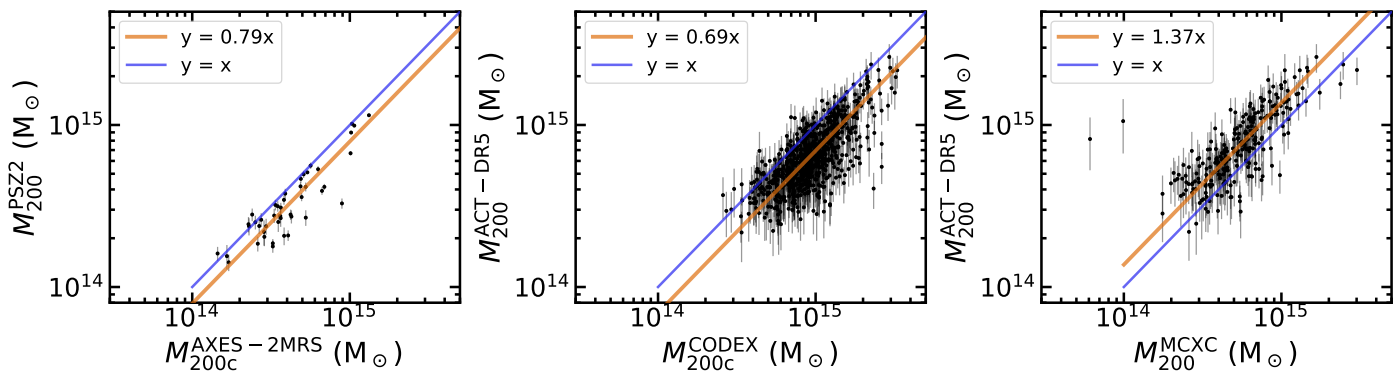


Fig. 2. Mass comparison examples. From left to right we compare PSZ2 to AXES-2MRS, ACT-DR5 to CODEX, and ACT-DR5 to MCXC mass estimates. Points with errorbars are all clusters in common between each pair of catalogues, whether part of CHANCES or not. We omit horizontal errorbars for clarity. Thin blue lines show $y = x$ while thick orange lines show least-squares linear relations, as given in the legends, ignoring horizontal uncertainties. These fits correspond to the adopted normalizations discussed in Section 3 and listed in Tables 1 and 2.

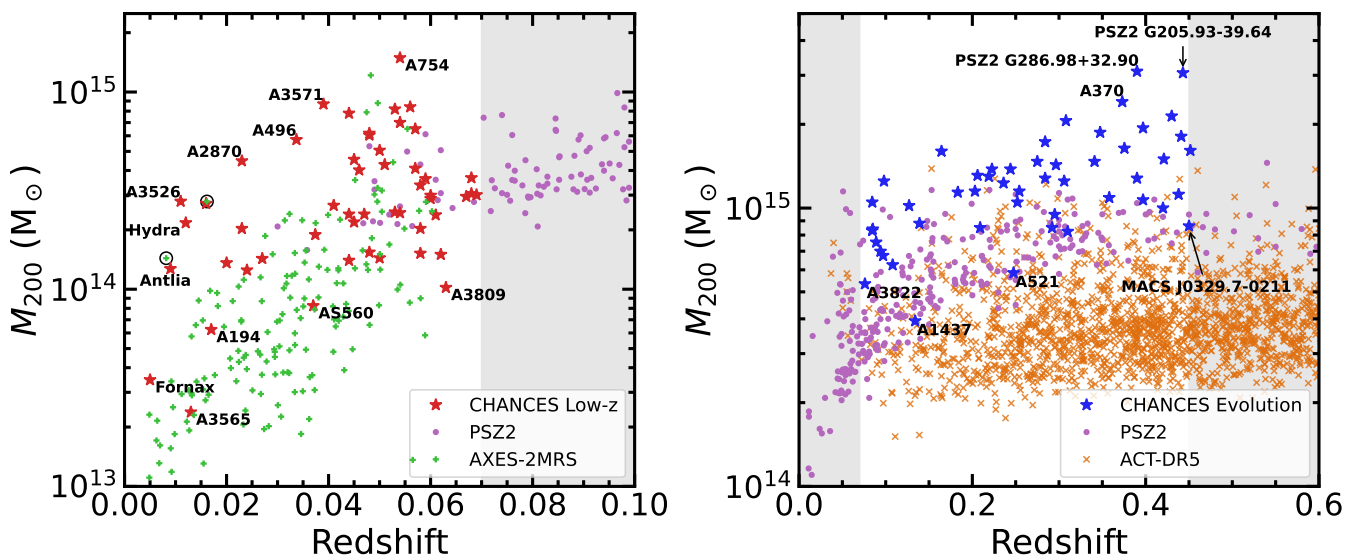


Fig. 3. CHANCES cluster samples (stars) in context. Left: Low- z subsurvey, excluding clusters in the Shapley and Horologium-Reticulum superclusters, compared with southern (i.e., $\text{Dec} < +5^\circ$) clusters in AXES-2MRS and PSZ2. Right: Evolution subsurvey, compared with southern clusters in PSZ2 and ACT-DR5. In both cases we remove duplicate clusters by only keeping the higher-priority mass estimate (see Section 3). We give the names of the least and most massive clusters in each sample, as well as some well-known clusters. In the left panel we also mark with black circles the two lowest-redshift $M_{200} > 10^{14} M_\odot$ AXES-2MRS clusters which are not part of CHANCES, namely NGC 5044 at $z = 0.008$ and Abell 3627 at $z = 0.016$ (which happens to have the same mass and redshift as Abell 3574); see text for details. In the right panel we also highlight MACS J0329.7–0211 which is the only Evolution cluster not in PSZ2. The redshift range of each CHANCES subsurvey is shown with the white background. CHANCES cluster masses correspond to those listed in Tables A.1 and A.2.

combine several cluster surveys, it is important to homogenize their mass estimates to provide uniformity. We emphasize here that the goal of this exercise is not to obtain accurate and precise mass estimates based on all the available data for each cluster but to establish a preliminary mass scale from which to obtain an estimate of r_{200} , which is used to define the extent of our target galaxy catalogues.

We retrieved mass estimates from various surveys and applied a normalization factor to each one to ensure statistical consistency. Because of different assumptions in estimating masses in each of the catalogues, this is preferable to combining masses from different catalogues. In order to estimate the normalization factors, we match clusters across catalogues with a $5'$ matching radius and a maximum redshift difference of 10%. The former matches the PSZ2 beam size and is small compared to the extent of Low- z clusters, while the latter allows photometric redshift errors, and we have tested that more stringent matching criteria

do not change the outcome. As a reference scale for the Low- z subsurvey masses we used the weak lensing mass estimates from MENeCS (Herbonnet et al. 2020), while for the Evolution subsurvey we use the masses derived from ACT-DR5 SZ effect mass estimates, which have been normalized to match the scale of weak lensing mass estimates as described in Hilton et al. (2021)⁵. While MENeCS masses are given as M_{200} , ACT-DR5 masses are given as M_{500} . We convert these, and other mass definitions as appropriate, to M_{200} using colossus⁶ (Diemer 2018), assuming an NFW profile (Navarro et al. 1996) with the Ishiyama et al. (2021) mass-concentration relation.

We show examples of cross-matched catalogues and the resulting mass normalizations in Figure 2, and summarize the normalizations applied to each external catalogue in Tables 1 and 2. We define the ‘‘CHANCES mass’’ of each CHANCES cluster

⁵ That is, we use the $M500cCa1$ column.

⁶ <https://bdiemer.bitbucket.io/colossus/>

following the order in [Tables 1](#) and [2](#) for the Low- z and Evolution samples, respectively. The last column in each table lists the number of clusters whose masses come from that particular catalogue, while the previous column includes clusters in common with higher-priority catalogues. This means, for instance in the case of Low- z , that all five clusters in MENeCS are assigned the MENeCS masses, the 13 AXES-2MRS clusters not in MENeCS are assigned the AXES-2MRS mass multiplied by 0.88, and so on. We only consider AXES-2MRS and AXES-LEGACY for clusters at $z < 0.04$, as discussed in [Section 2.1](#).

When there are not enough cross-matches between a particular catalogue and the reference catalogue we apply successive normalizations. For example, the normalization of 0.86 for AXES-2MRS (and AXES-LEGACY) comes from the combination of $M_{200}^{\text{PSZ2}} = 0.79M_{200}^{\text{AXES-2MRS}}$ (shown in the left panel of [Figure 2](#)) and $M_{200}^{\text{ACT-DR5}} = 1.09M_{200}^{\text{PSZ2}}$ (not shown). Fits are performed through weighted least squares accounting only for uncertainties in the dependent quantity for simplicity. The ACT-DR5 and the two SPT catalogues have been shown to be consistent with each other and with weak lensing mass estimates ([Bleem et al. 2020](#); [Hilton et al. 2021](#)), so we set all these normalizations to one.

The two outliers in the right panel of [Figure 2](#) are Abell 536 at $z = 0.040$ and Abell S560 at $z = 0.037$, with ACT-DR5 masses 11 and 13 times the MCXC masses, respectively. At such low redshifts the ACT-DR5 catalogue is highly incomplete and therefore it is expected that some clusters are up-scattered due to either statistical or intrinsic noise, and this may raise concerns about using ACT-DR5 in the Low- z sample. Reassuringly, the two Low- z clusters assigned ACT-DR5 masses – Abell 3667 ($z = 0.053$) and Abell 4059 ($z = 0.048$) – have mass estimates from ACT-DR5, PSZ2, MCXC, AXES-LEGACY, and WINGS, with standard deviations of 16% and 29%, respectively, so the catalogue choice has only a small impact on the assigned r_{200} (namely, 5% and 10%, respectively).

There are two exceptions to the above scheme, and both pertain to the Low- z subsurvey. The first is Abell 3395, which is a well-known merging system, in addition to being in close proximity to Abell 3391 (e.g. [Reiprich et al. 2021](#); [Dietl et al. 2024](#); [Veronica et al. 2024](#)). Abell 3395 has a mass estimate from the WINGS survey of $M_{200} = 2.9 \times 10^{15} M_{\odot}$ ([Moretti et al. 2017](#)), while all ICM-based estimates suggest $M_{200} \sim 5 \times 10^{14} M_{\odot}$ ([Piffaretti et al. 2011](#); [Planck Collaboration 2016](#); [Bulbul et al. 2024](#); [Damsted et al. 2024](#)). Because velocity dispersion-based masses are known to be highly biased for merging clusters (as was indeed pointed out by [Moretti et al. 2017](#)), we choose to instead use the PSZ2 mass for Abell 3395, $M_{200} = 5.1 \times 10^{14} M_{\odot}$. The other exception is Abell 3490, for which we use the rescaled AXES-LEGACY mass even though it is at $z = 0.069$, because it is not matched to any other catalogue. The resulting mass estimates for each cluster, and the associated r_{200} , are listed in [Tables A.1](#) and [A.2](#).

We show the CHANCES clusters in mass–redshift space in [Figure 3](#). We place the sample of each subsurvey in context by comparing them to the mass and redshift distributions of southern (i.e., $\text{Dec} < +5^{\circ}$) clusters in PSZ2 and AXES-2MRS (Low- z , left panel) and PSZ2 and ACT-DR5 (Evolution, right panel). We remove duplicates from [Figure 3](#) by matching clusters as described above (a matching radius of $5'$ and a redshift difference of $< 10\%$), following the priority scheme already described. That is, in the left panel we only show as green crosses AXES-2MRS clusters which are not in CHANCES and only show as purple circles PSZ2 clusters which are neither in AXES-2MRS nor CHANCES. Analogously for the Evolution

Table 1. Mass sources for the Low- z subsurvey, ordered by priority. Columns are: (1) correction factor applied to masses provided by the survey, according to the comparison described in [Section 3](#); (2) total number of CHANCES clusters in each catalogue; and (3) how many clusters get their CHANCES mass estimates from each source.

Survey	(1) Correction factor	(2) No. of clusters	(3) Source for
MENeCS ^a	1	5	5
AXES-2MRS ^b	0.86	23	13
AXES-LEGACY ^c	0.86	36	1
ACT-DR5 ^d	1	5	2
SPT-ECS ^e	1	1	0
SPT-SZ ^f	1	2	1
WINGS ^g	0.76	18	13
MCXC ^h	1.37	43	13
PSZ2 ⁱ	1.09	27	2
CODEX ^j	0.69	34	1

Notes. ^(a) [Herbonnet et al. \(2020\)](#) ^(b) [Khalil et al. \(2024\)](#). Used only for clusters at $z \leq 0.04$. ^(c) [Finoguenov et al. \(in prep\)](#). Used only for clusters at $z \leq 0.04$, except for Abell 3490 ($z = 0.069$) which is not matched in any other catalogue. ^(d) [Hilton et al. \(2021\)](#) ^(e) [Bleem et al. \(2020\)](#) ^(f) [Bleem et al. \(2015\)](#) ^(g) [Moretti et al. \(2017\)](#) ^(h) [Piffaretti et al. \(2011\)](#) ⁽ⁱ⁾ [Planck Collaboration \(2016\)](#) ^(j) [Damsted et al. \(2023\)](#)

Table 2. Mass sources for the Evolution sub-survey, ordered by priority. See [Table 1](#) for details and additional references.

Survey	Correction factor	No. of clusters	Source for
LoCuSS ^a	1	4	4
MENeCS	1	11	8
CoMaLit ^b	1	25	14
ACT-DR5	1	34	14
SPT-ECS	1	14	3
SPT-SZ	1	12	2
PSZ2	1.09	49	6
CODEX	0.69	40	0
MCXC	1.37	40	0

Notes. ^(a) [Okabe & Smith \(2016\)](#). Does not contain any clusters in the Low- z redshift range. ^(b) [Sereno \(2015\)](#)

sample in the right panel. As shown in the left panel of [Figure 3](#), CHANCES includes all massive clusters at $z < 0.02$ in the Southern hemisphere, with two exceptions. The first is known simply as NGC 5044; at $z = 0.009$, it is part of the HI-FLUCGS survey derived from ROSAT observations ([Reiprich & Böhringer 2002](#)). NGC 5044 is within LSDR10 but does not have r -band observations, which we require for photometric redshift estimation. The second exception is Abell 3627 at $z = 0.016$, which we exclude because of its low Galactic latitude, $b = -7^{\circ}$.

At $z > 0.04$, CHANCES clusters cover the entire mass range probed by AXES and PSZ2, while at lower redshifts the selection is biased toward high-mass systems. In contrast, with a few exceptions, the Evolution sample specifically targets the most massive systems, although as mentioned we enforced homogeneous coverage of the full Evolution redshift range. Such a continuous sampling of the most massive clusters from $z = 0$ to $z = 0.45$ is not designed to track the evolution of clusters – it is evident that clusters in the Low- z sample are not the descendants

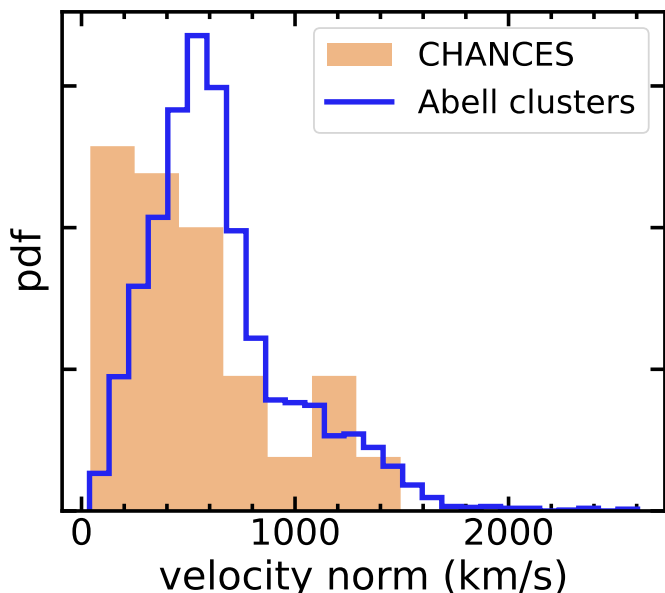


Fig. 4. Three-dimensional peculiar velocity norm distribution of CHANCES clusters, compared to all Abell clusters with known redshifts. These have been reconstructed by Dupuy & Courtois (2023) from distances estimated by Cosmicflows-4 (Courtois et al. 2023). Bin sizes have been chosen using Knuth (2006)’s rule. CHANCES clusters tend to reside in regions with small peculiar velocities, suggesting they are preferentially sites where matter from the large scale structure is falling toward.

of clusters in the Evolution sample. Instead, by targeting the entire volume around each cluster that is detached from the Hubble flow, we will learn what is the impact of the time of arrival on the infall patterns and their consequences on galaxy evolution, i.e., the Butcher-Oemler effect (Butcher & Oemler 1984). The superclusters then provide a natural extension by probing larger-scale environments including the full region that will become detached from the Hubble-Lemaître flow in the distant future (Dünner et al. 2006; Araya-Melo et al. 2009).

We expand upon the previous point by looking at the reconstruction of peculiar velocities of CHANCES clusters. These peculiar velocities were derived by Dupuy & Courtois (2023) by reconstructing the large-scale density using the distances estimated by the Cosmicflows-4 project (Courtois et al. 2023). Peculiar velocities trace the location in the large-scale structure of the Universe: generally speaking, large peculiar-velocity structures are falling towards small peculiar-velocity structures. Figure 4 shows the distribution⁷ of peculiar velocities of all CHANCES clusters (excluding superclusters), compared to all Abell clusters with known redshifts.⁸ CHANCES clusters cover a large range of peculiar velocities. Some clusters have peculiar velocities as low as 100 km s^{-1} , suggesting they are major local attractors, while others have peculiar velocities well above 1000 km s^{-1} , implying they are influenced by a more dominant structure in the cosmic web. This is expected from the broad mass range covered particularly by the Low- z subsurvey, and offers yet another aspect whose impact on galaxy evolution will be uniquely assessed by CHANCES.

⁷ We define bin widths using Knuth (2006)’s rule, which optimizes the bin size of a piecewise-constant probability distribution in a Bayesian framework. We use the implementation in `astropy.visualization`.

⁸ As listed in the NASA/IPAC Extragalactic Database, <http://ned.ipac.caltech.edu/>.

4. Cluster environments: A sneak peek

4.1. A preliminary census of infalling structures around CHANCES clusters

One of the primary goals of CHANCES is to study pre-processing of galaxies prior to cluster infall. It is thus important to characterize not only the main clusters but nearby structures. As a proof of concept, we explore the network of groups⁹ around CHANCES clusters using the redMaPPer (Rykoff et al. 2014) group catalogue constructed using the LSDR10. This catalogue was constructed by Kluge et al. (2024) to provide targets for the 4MOST eROSITA Galaxy Cluster Redshift Survey (Finoguenov et al. 2019) following the strategy described in Clerc et al. (2020). redMaPPer identifies associations of red galaxies and calculates the richness, λ , as the total membership probability across all galaxies within a richness-dependent cluster radius which is of order 1 Mpc. When the central galaxy in a redMaPPer group has a literature spectroscopic redshift, the spectroscopic redshift is assigned to the cluster; otherwise the cluster retains its red-sequence photometric redshift (Rykoff et al. 2014). For reference, redMaPPer redshift errors are typically 5–8%, which translates into an error in the velocity of roughly $1000\text{--}2000 \text{ km s}^{-1}$ at $z = 0.1$. By construction, this catalogue does not contain systems lacking a developed red sequence. Such a selection effect only impacts low-mass systems, and overcoming it requires the spectroscopic completeness that CHANCES will provide. We consider all redMaPPer groups within $5r_{200}$ of each CHANCES clusters and with peculiar velocities $|v_{\text{pec}}| = c|z - z_{\text{cl}}|/(1 + z_{\text{cl}}) < 8000 \text{ km s}^{-1}$, where z_{cl} is the redshift of the CHANCES cluster as listed in Tables A.1 and A.2. For the purpose of this demonstration we also calculate each CHANCES cluster’s one-dimensional velocity dispersion given M_{200} using the relation by Munari et al. (2013). We call this velocity dispersion σ_{main} .

Figure 5 shows the redMaPPer groups thus selected around example Low- z and Evolution clusters. Each coloured circle shows a redMaPPer group, with circle size equal to each group’s r_{200} . Filled circles correspond to systems with $|v_{\text{pec}}| < 3\sigma_{\text{main}}$. In order to estimate each redMaPPer group’s r_{200} we multiply the redMaPPer richness, λ , by 1.21 to match the DES richness scale (Kluge et al. 2024) and use the relation between λ and weak lensing mass derived by McClintock et al. (2019) for DES clusters.¹⁰ There are a total 1,406 redMaPPer groups thus selected – an average 13.5 redMaPPer groups within $5r_{200}$ of each CHANCES cluster. We then identify the most massive redMaPPer group within the nominal CHANCES r_{200} (cf. Tables A.1 and A.2) as the CHANCES cluster itself. Automatic cluster finding is notoriously difficult at very low redshift where the mean separation between galaxies is several arcmin on the sky. Indeed, we find that we assign a redMaPPer group with the main CHANCES cluster in 30 Low- z clusters, all at $z > 0.037$, while the rest – all at $z < 0.048$ – do not have any redMaPPer matches within r_{200} . One such example is Abell 1644, shown in the top-left panel of Figure 5. Some clusters, however, may be matched to the wrong main cluster, such as in the case of Abell 1520 in the top-centre panel of Figure 5. All Evolution clusters have a

⁹ Traditionally the division between cluster and group is set by a mass threshold, typically around $10^{14} M_{\odot}$. In an attempt to reduce confusion and redundancy, in this section we use both terms hierarchically, i.e., CHANCES clusters are surrounded by redMaPPer groups, regardless of mass.

¹⁰ We convert from $M_{200\text{m}}$ estimated from the McClintock et al. (2019) relation to M_{200c} as above, using the mass-concentration relation of Ishiyama et al. (2021) as implemented in `colossus` (Diemer 2018).

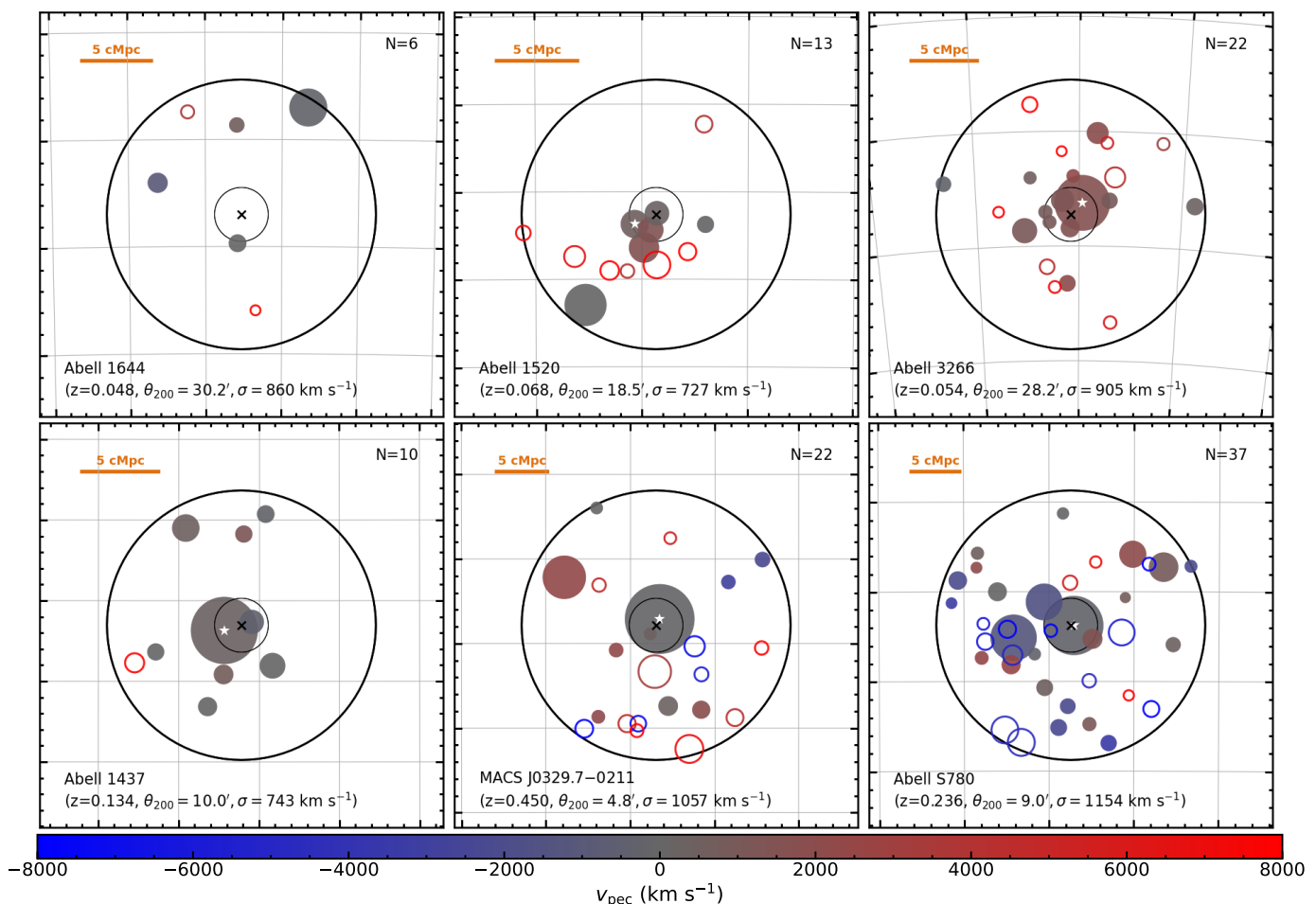


Fig. 5. Infalling structures in example CHANCES Low- z (top) and Evolution (bottom) clusters, as traced by associations of red galaxies identified with redMaPPer within $8,000 \text{ km s}^{-1}$ of each CHANCES cluster’s nominal redshift. Filled circles correspond to redMaPPer groups with velocities within three times the CHANCES velocity dispersion. For each subsurvey we show a cluster with a small (left), typical (middle), and large (right) number of redMaPPer subclusters. The concentric black cross and empty thin and thick circles mark each CHANCES cluster’s centre, r_{200} , and $5r_{200}$, respectively. Coloured circle sizes correspond to each group’s r_{200} based on its richness. The colour scale shows the peculiar velocity with respect to the main cluster. When present, the redMaPPer system associated with the main CHANCES cluster is shown with a white star. In the bottom of each panel we list each cluster’s redshift, angular size corresponding to r_{200} , and richness-derived velocity dispersion. Numbers on the top right corners correspond to the number of redMaPPer groups and clusters shown, and the orange bars on the top left corners indicate 5 comoving Mpc at each cluster’s redshift.

redMaPPer match, except for RXJ 1347.5–1144 which is not within the LSDR10 redMaPPer footprint. As expected, some CHANCES clusters contain a wealth of infalling groups, although in others this is not apparent from the redMaPPer catalogue. This may be due either to incompleteness in the redMaPPer catalogue (e.g., because such low-mass systems might not contain a red sequence) or because some CHANCES clusters really reside in regions devoid of significant galaxy overdensities, a question only the high spectroscopic completeness provided by CHANCES will answer.

We now look at the statistical properties of the redMaPPer sample and its relation to CHANCES clusters. In Figure 6 we show the line-of-sight velocity against projected cluster-centric distance, typically referred to the phase-space diagram, for redMaPPer systems surrounding CHANCES clusters. Phase-space diagrams are commonly used to infer the infall history of galaxy populations within clusters (e.g., Oman et al. 2013; Muzzin et al. 2014; Haines et al. 2015; Jaffé et al. 2015). As with galaxies, the phase-space diagram of infalling groups reveals details about their infall history (e.g., Jaffé et al. 2016; Einasto et al. 2018; Haines et al. 2018; Piraino-Cerda et al. 2024). Each point

in Figure 6 is a redMaPPer group near a CHANCES cluster. The velocities in Figure 6 are affected by uncertainties in the cluster redshifts, which are derived from the mean colour of the red sequence (Rykoff et al. 2014) and therefore to first order scale as $\sigma_z \propto \lambda^{-1/2}$. The right panel shows that redMaPPer redshifts tend to be biased high, particularly for the Low- z sample; this is a consequence of the above redshift errors, the small cluster redshifts, and the strict $z > 0$ prior.¹¹ Nevertheless there is a clear overdensity of groups around $v_{\text{pec}} = 0 \text{ km s}^{-1}$. The main CHANCES clusters are excluded from Figure 6 following the associations described above. However, some redMaPPer groups are located right at the CHANCES cluster centres. These are cases where the simple association above has evidently failed, possibly due to the fragmentation of the system by redMaPPer (e.g., Abell 1520 and Abell 1437 in Figure 5). Once again we treat such failures as a nuisance in the context of the proof of concept presented here. The more massive systems do cluster around $v_{\text{pec}} = 0$, suggesting that the above photometric redshift

¹¹ Since we use spectroscopic redshifts from the literature for the main CHANCES clusters, they are not subject to this effect.

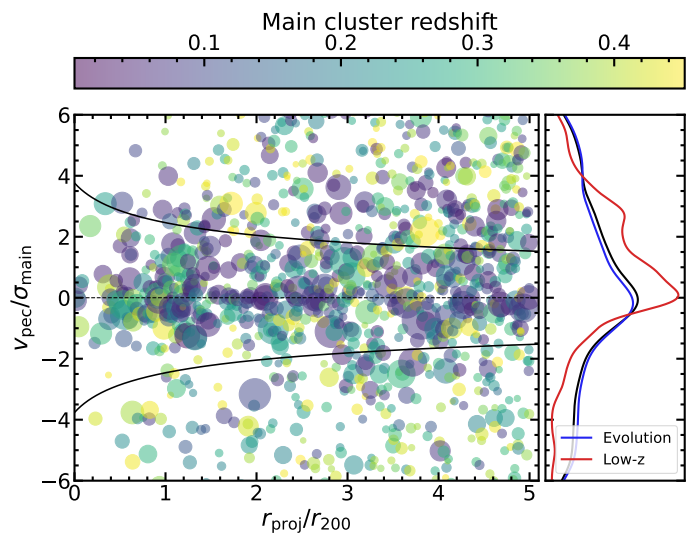


Fig. 6. Line-of-sight velocity vs. projected distance of redMaPPer groups around all CHANCES clusters. Each circle is a redMaPPer group and has a radius proportional to the group’s richness-derived r_{200} in units of each CHANCES cluster’s r_{200} , and is colour-coded by redshift. redMaPPer groups corresponding to the main CHANCES cluster are excluded from this plot. The black solid lines show the escape velocity for a NFW profile, which in these units has negligible dependence on mass and redshift; redMaPPer groups with larger peculiar velocities are expected to be unbound from the respective CHANCES cluster. The right panel shows kernel density estimates of the normalized peculiar velocity distributions, using a Gaussian kernel with a width of 0.2, for the Low-z (red) and Evolution (blue) samples, as well as the combined distribution (black). Note that some redMaPPer groups have spectroscopic redshifts but others have photometric ones; all of them are included in this figure.

bias affects mostly low-mass systems. This is expected, since they have fewer galaxies from which to calculate the mean cluster redshift and are thus subject to larger statistical uncertainties.

Figure 6 shows that many of the clusters selected with this simple velocity cut have peculiar velocities much larger than the escape velocity, $v_{\text{esc}}(r) = \sqrt{2|\phi(r)|}$, where ϕ is the potential of an NFW profile for illustration¹² (e.g., Miller et al. 2016). Such objects are thus not falling into the main clusters, although some of them could be part of the same large-scale structure. Of course, a stricter velocity cut than the simple $v_{\text{pec}} < 8000 \text{ km s}^{-1}$ would remove many of the unrelated systems. Since we are using photometric redshifts here it is not justified to delve further into this point; CHANCES will enable a detailed assessment of the filamentary structure, including embedded groups, associated with clusters in our sample. In-depth analyses of the filamentary structure around CHANCES clusters from the available photometric data will be presented in Baier et al. in prep. and Piraino-Cerda et al. in prep. Combined with the optical properties of the member galaxies, both from ancillary imaging and the CHANCES spectra, as well as with X-ray and SZ measurements of the intragroup medium properties (in some cases individually and in some cases through stacking), CHANCES will allow us to closely link the infall history of galaxies falling into CHANCES clusters as members of groups or as part of the filamentary network but not a group, as well as with “field” galaxies outside this network.

¹² For simplicity we use the three-dimensional distance in the calculation.

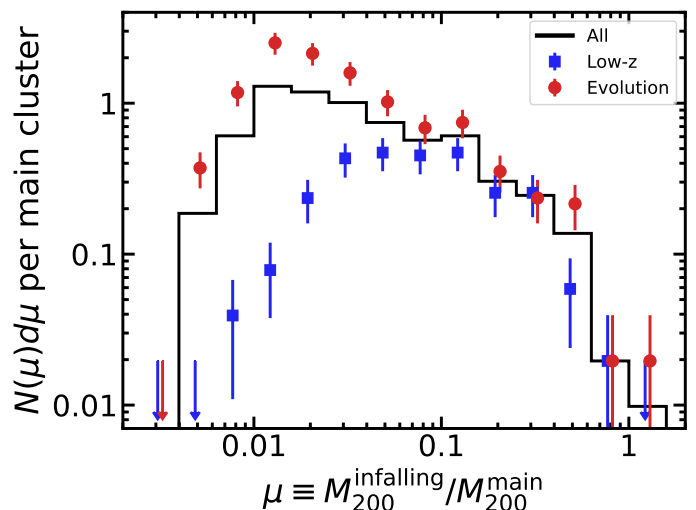


Fig. 7. Mass functions of infalling groups for the Low-z (blue) and Evolution (red) samples, as well as both combined (black), including only redMaPPer groups with $|v_{\text{pec}}| < 3\sigma_{\text{main}}$. Differential counts have been normalized to the number of CHANCES clusters in each sample and have not been corrected for incompleteness. Errorbars are Poisson uncertainties and arrows are 1σ upper limits. We show the full sample as a histogram and omit errorbars to avoid cluttering. Blue and red data points are slightly shifted horizontally for clarity.

Table 3. Multiple-cluster systems, overlapping both on the sky and in redshift space.

CHANCES clusters	Redshift
Antlia / Hydra	0.012 / 0.012
A119 / A147 / A168	0.044 / 0.044 / 0.044
A754 / A780	0.054 / 0.057
A1631 / A1644	0.047 / 0.048
A1650 / A1651	0.085 / 0.085
A2717 / A4059	0.050 / 0.048
A2870 / A2877	0.023 / 0.024
A3651 / A3667	0.060 / 0.053

Finally, in Figure 7 we show the mass function of redMaPPer groups with $|v_{\text{pec}}| < 3\sigma_{\text{main}}$ (a common first selection of member galaxies within clusters), again taking the richness-derived masses and excluding main CHANCES clusters. We show the mass function in units of the main cluster mass as listed in Tables A.1 and A.2, whereas the masses of infalling systems are the richness-derived masses, an inconsistency which we ignore for the purpose of this discussion. Interestingly, both the Low-z and Evolution populations follow the same mass distribution for mass ratios $\mu \equiv M_{200}^{\text{infalling}}/M_{200}^{\text{main}} > 0.1$, suggesting a lack of evolution of the high-mass end of the infall mass function over the past 5 Gyr. At lower mass ratios the Low-z distribution remains constant until $\mu \sim 0.03$ and then decreases, while the Evolution distribution continues to grow until $\mu \sim 0.01$ and then drops abruptly. The most natural interpretation for this change in behaviour is incompleteness of the redMaPPer catalogue at low masses: the points at which both distributions turn over correspond approximately to $M_{200}^{\text{infalling}} \sim 10^{13} M_{\odot}$, i.e., at a mass regime where we do not expect the red sequence to be as dominant as required by redMaPPer.

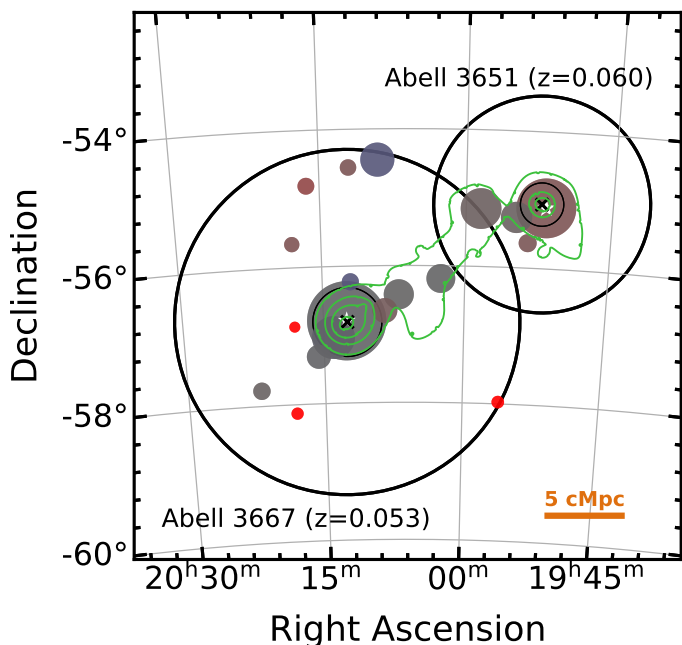


Fig. 8. The Abell 3651/3667 system as an example of overlapping CHANCES clusters (see Section 4.2). Symbols and colours are the same as in Figure 5, except we do not discriminate redMaPPer systems according to the CHANCES velocity dispersions. Circle colours are with respect to a reference $z = 0.056$, and the orange bar at the bottom right shows 5 comoving Mpc at the same redshift. Green contours show the eROSITA detection of hot gas within and between the clusters (Dietl et al. 2024).

4.2. Multiple-cluster systems

In addition to the rich array of infalling groups, a few CHANCES clusters are associated with each other – they overlap with other CHANCES clusters both in the sky and in redshift. We define a multiple-cluster system of clusters as one where the $5r_{200}$ circles of multiple clusters overlap. These systems are listed in Table 3, and will offer an even larger view of the cosmic web surrounding massive clusters and serve as an intermediate regime between single CHANCES clusters and superclusters. All of these overlapping systems are part of the Low- z subsurvey, except for Abell 1650/1651.

We show as an example the Abell 3651/3667 system in Figure 8. [Arp & Russell \(2001\)](#) recognized a possible connection between these two clusters based on the distributions of galaxies in optical images and of X-ray point sources from ROSAT data. [Dietl et al. \(2024\)](#) detected a bridge of X-ray emission connecting these two clusters in the eROSITA X-ray images, which is nicely traced by the structure of redMaPPer groups shown in Figure 8. Furthermore, like many other CHANCES clusters, Abell 3667 is a well-known merging system with a spectacular morphology at radio wavelengths tracing non-thermal phenomena in the ICM ([de Gasperin et al. 2022](#)). In combination with ICM data, CHANCES will reveal the full extent of the network connecting these two clusters and the others in Table 3.

4.3. Superclusters

We end this sneak peek by showing in Figure 9 all redMaPPer clusters within and around both supercluster regions. We illustrate the hierarchy of clusters in each supercluster by defin-

ing primary clusters as those which are the most massive system within their $5r_{200}$ and are not within the $5r_{200}$ of any more massive cluster. All clusters that are not primaries are labelled as secondary. Considering only the regions to be surveyed by CHANCES, there are 21 primary and 53 secondary clusters in Shapley and 44 primary and 92 secondary clusters in Horologium-Reticulum. Although we draw full circles around all primary clusters within the survey regions in Figure 9, only the area within the thick polygons will be observed. The exceptions are the two clusters shown with blue crosses in Figure 9: Abell 3571 in Shapley and Abell 3266 in Horologium-Reticulum. In these cases CHANCES will cover the entire $5r_{200}$ area, adding the non-overlapping area to the supercluster coverage. The difficulty of characterizing low-redshift structures with photometric redshifts is again highlighted in the lack of a match in the redMaPPer catalogue for Abell 3571: this cluster is at $z = 0.039$ yet the only $z < 0.2$ redMaPPer cluster within $20'$ has $z_{\text{phot}} = 0.19$ and $\lambda = 5$. Evidently, the absence of Abell 3571 from the redMaPPer catalogue has an impact on our census of primary and secondary clusters, highlighting once again the need for CHANCES spectroscopy.

As mentioned in Section 2.1.2, Abell 3574 is located just north of Abell 3571, but at $z = 0.016$ it is at a significantly lower redshift than the Shapley supercluster (and Abell 3571). This means target overlap will be minimal in this case, even though both targets (i.e., Abell 3574 and the Shapley supercluster) overlap in the sky. A similar situation occurs in Horologium-Reticulum, which has significant overlap with the Fornax cluster (whose $5r_{200}$ reaches as far south as -58°) in the sky but not in redshift.

5. Summary

We present the cluster sample for CHANCES, the Chilean Cluster galaxy Evolution Survey, one of 18 4MOST Public Surveys which will use the 4MOST Spectroscopic Survey Facility on the VISTA 4m telescope over the next five years. CHANCES will obtain spectra for 500,000 galaxies out to $5r_{200}$ around galaxy clusters at $z < 0.45$ (Figure 1) in three different regimes:

- (i) $m^* > 10^{8.5} M_\odot$ galaxies around 50 clusters at $z < 0.07$ covering an order of magnitude in cluster masses (Figure 3, left panel);
- (ii) $m^* > 10^{8.5} M_\odot$ galaxies in large contiguous regions over a total of 353 deg^2 covering the Shapley ($z = 0.048$) and Horologium-Reticulum ($z = 0.060$) superclusters (Figure 9);
- (iii) $m^* > 10^{10} M_\odot$ galaxies around 50 of the most massive clusters at $0.07 < z < 0.45$ (Figure 3, right panel).

Points (i) and (ii) comprise the Low- z subsurvey (Section 2.1) while point (iii) refers to the Evolution subsurvey (Section 2.2). Clusters in the Low- z subsurvey were selected by combining the AXES-2MRS catalogue ([Khalil et al. 2024](#)) at $z < 0.04$ with the WINGS survey at $0.04 < z < 0.07$ ([Fasano et al. 2006](#)). Clusters in the Evolution subsurvey were selected as the most massive southern clusters from the 2nd Planck SZ-selected cluster catalogue ([Planck Collaboration 2016](#)) in five bins across $0.07 < z < 0.45$ to ensure uniform redshift coverage. With the exception of the Antlia cluster at $z = 0.0087$, to select clusters in both subsurveys we require multi-band optical imaging from DECaLS DR10 for uniform photometry and astrometry.

We produced consistent mass estimates for all clusters by rescaling masses from a number of literature sources (Figure 2)

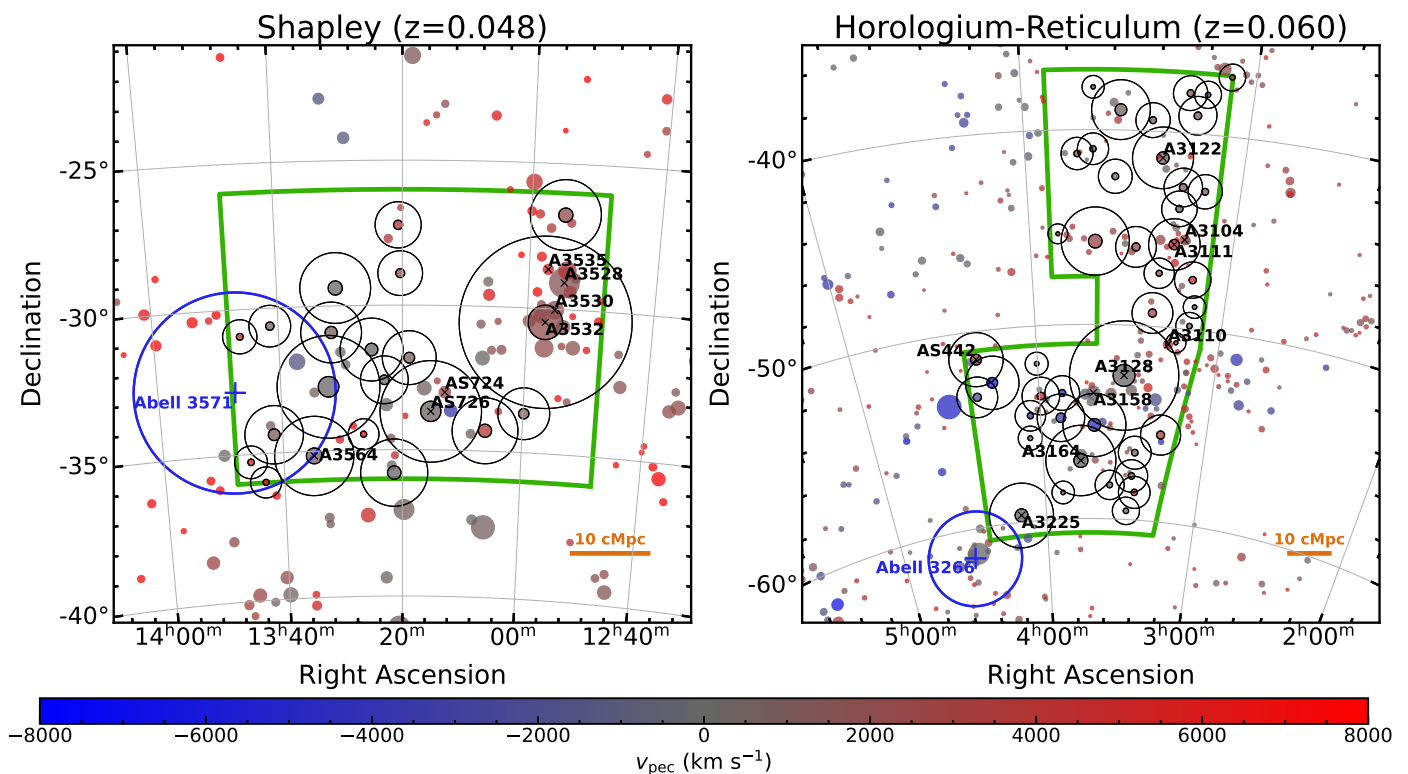


Fig. 9. Optical groups and clusters identified with redMaPPer, within and around the Shapley (left) and Horologium-Reticulum (right) superclusters. Colours represent velocity with respect to the mean supercluster redshift (titles). Sizes are equal to r_{200} determined through the redMaPPer richness. Coloured circles with black outlines are primary clusters (only shown within the supercluster regions); those without the black outline are secondary clusters or are outside the CHANCES supercluster survey areas, which are marked with green polygons. For primary clusters we also show $5r_{200}$ with a black circle. The blue crosses and circles mark clusters Abell 3571 (left) and Abell 3266 (right), which are at the supercluster redshifts but are targeted individually as CHANCES main clusters. We also mark the most massive redMaPPer systems associated with Abell clusters with black crosses (not all of which are primaries).

in order to obtain mass estimates consistent with weak lensing measurements from MENEaCS (Herbonnet et al. 2020) and LoCuSS (Okabe & Smith 2016), which are in turn consistent with a number of other weak lensing mass estimates, as well as calibrated SZ-based mass estimates from ACT and SPT.

As a proof of concept for some of the main CHANCES goals, we use the redMaPPer red-sequence catalogue ran on the LSDR10 imaging data to present a preliminary census of groups surrounding the CHANCES clusters (Figures 5 and 8) as well as the cluster and group distribution composing the CHANCES superclusters (Figure 9). Peculiar velocity reconstruction suggest CHANCES clusters tend to reside in local attractors, although they cover a wide range of large-scale environments. We also present preliminary measurements of the stacked phase-space (Figure 6) and mass function (Figure 7) of groups associated to CHANCES clusters. The unique wide coverage and high completeness of CHANCES will provide an unprecedented view of the evolution of galaxies and the growth of structure facilitated by the cosmic web. Beyond our census of infalling groups, CHANCES will reveal the full extent of the multi-phase cosmic web surrounding massive clusters, including the sheets and filaments that funnel these groups into their more massive neighbours.

In a series of forthcoming papers we will present in detail the target selection procedure, which involves assessing cluster membership from photometric data, as well as thorough analyses of the substructure and large-scale structure based on the resulting target catalogues.

Acknowledgements. We thank Jakob Dietl for sharing the eROSITA contours for the Abell 3651/3667 system. CS, YJ, RD, and AM acknowledge support from the Agencia Nacional de Investigación y Desarrollo (ANID) through Basal project FB210003. CS acknowledges support from FONDECYT Iniciación grant no. 11191125. AF thanks FINCA, USM, Uda for the travel support. CPH acknowledges support from ANID through Fondecyt Regular 2021 project no. 1211909. YJ acknowledges support from FONDECYT Regular grants no. 1241426 and 1230441. BMA acknowledges the Universidad de Atacama PhD Scholarship and the Fondecyt Regular 2021 Grant of Dr. Christopher P. Haines, PhD Supervisor, for the expenses to successfully conduct this research. R.D. gratefully acknowledges support by the ANID BASAL project FB210003. E. R. V. L. acknowledges the financial support given by Coordenação de Aperfeiçoamento de Pessoal de Nível Superior (CAPES, grant 88887.470064/2019-00) and Conselho Nacional de Desenvolvimento Científico e Tecnológico (CNPq, grant 169181/2017-0). CL-D acknowledges a grant from the ESO Comite Mixto 2022. H.M.H. acknowledges support from National Fund for Scientific and Technological Research of Chile (FONDECYT) through grant no. 3230176. AM acknowledges support by the FONDECYT Regular grant 1212046 and funding from the Max Planck Society through a “PartnerGroup” grant and the HORIZON-MSCA-2021-SE-01 Research and Innovation Programme under the Marie Skłodowska-Curie grant agreement number 101086388. PA-A thanks the Coordenação de Aperfeiçoamento de Pessoal de Nível Superior – Brasil (CAPES), for supporting his PhD scholarship (project 88882.332909/2020-01). M.A-F acknowledges support from ANID FONDECYT iniciación project 11200107 and the Emergia program (EMERGIA20_38888) from Consejería de Universidad, Investigación e Innovación de la Junta de Andalucía. ANID / Subdirección de Capital Humano / Doctorado Nacional / 2023 - 21231017. C. R. Bom acknowledges the financial support from CNPq (316072/2021-4) and from FAPERJ (grants 201.456/2022 and 210.330/2022) and the FINEP contract 01.22.0505.00 (ref. 1891/22). HMC acknowledges support from the Institut Universitaire de France and from Centre National d’Etudes Spatiales (CNES), France. GD acknowledges support by UKRI-STFC grants: ST/T003081/1 and ST/X001857/1. AD is supported by a KIAS Individual Grant PG 087201 at the Korea Institute for Advanced Studies. RFH acknowledge financial support from Consejo Nacional de Investigaciones Científicas y Técnicas (CONICET), Agencia I+D+i (PICT 2019–03299),

and Universidad Nacional de La Plata (Argentina). F.R.H. acknowledges support from FAPESP grants 2018/21661-9 and 2021/11345-5. E.I. acknowledge funding by ANID FONDECYT Regular 1221846. UK acknowledges financial support from the UK Science and Technology Facilities Council (STFC; grant ref: ST/T000171/1). ARL acknowledges financial support from CONICET, Agencia I+D+i (PICT 2019-03299) and Universidad Nacional de La Plata (Argentina). S.L. acknowledges support by FONDECYT grant 1231187. CMdO acknowledges funding of the S-PLUS project through FAPESP grant 2019/26492-3. LM acknowledge the support from PROYECTOS FONDO de ASTRONOMIA ANID – ALMA 2021 Code: ASTRO21-0007. DP acknowledges financial support from ANID through FONDECYT Postdoctorado Project 3230379. F.P.C. acknowledges financial support from Dirección de Postgrado (Universidad Técnica Federico Santa María, Chile) through Becas Internas para Doctorado y Magister Científico-Tecnológicos. RS acknowledges financial support from FONDECYT Regular 2023 project No. 1230441 and ANID - MILENIO NCN2024_112 - MINGAL (Millennium Nucleus for GALaxies). AVSC acknowledges financial support from CONICET, Agencia I+D+i (PICT 2019-03299) and Universidad Nacional de La Plata (Argentina). LSJ acknowledges the support from CNPq (308994/2021-3) and FAPESP (2011/51680-6). ET was supported by the Estonian Ministry of Education and Research (grant TK202), Estonian Research Council grant (PRG1006) and the European Union's Horizon Europe research and innovation programme (EXCOSM, grant No. 101159513).

References

- Alberts, S. & Noble, A. 2022, [arXiv:2209.02781](#), *Universe*, **8**, 554, From Clusters to Proto-Clusters: The Infrared Perspective on Environmental Galaxy Evolution
- Anand, A., Nelson, D., & Kauffmann, G. 2021, [arXiv:2103.15842](#), *MNRAS*, **504**, 65, Characterizing the abundance, properties, and kinematics of the cool circumgalactic medium of galaxies in absorption with SDSS DR16
- Araya-Melo, P. A., Reisenegger, A., Meza, A., van de Weygaert, R., Dünner, R., & Quintana, H. 2009, [arXiv:0809.1417](#), *MNRAS*, **399**, 97, Future evolution of bound superclusters in an accelerating Universe
- Arp, H. & Russell, D. 2001, *ApJ*, **549**, 802, A Possible Relationship between Quasars and Clusters of Galaxies
- Bahé, Y. M., McCarthy, I. G., Balogh, M. L., & Font, A. S. 2013, [arXiv:1210.8407](#), *MNRAS*, **430**, 3017, Why does the environmental influence on group and cluster galaxies extend beyond the virial radius?
- Bahé, Y. M., et al. 2019, [arXiv:1901.03336](#), *MNRAS*, **485**, 2287, Disruption of satellite galaxies in simulated groups and clusters: the roles of accretion time, baryons, and pre-processing
- Bertschinger, E. 1985, *ApJS*, **58**, 39, Self-similar secondary infall and accretion in an Einstein-de Sitter universe
- Bianconi, M., Smith, G. P., Haines, C. P., McGee, S. L., Finoguenov, A., & Egami, E. 2018, [arXiv:1710.04230](#), *MNRAS*, **473**, L79, LoCuSS: pre-processing in galaxy groups falling into massive galaxy clusters at $z = 0.2$
- Bleem, L. E., et al. 2015, [arXiv:1409.0850](#), *ApJS*, **216**, 27, Galaxy Clusters Discovered via the Sunyaev-Zel'dovich Effect in the 2500-Square-Degree SPT-SZ Survey
- Bleem, L. E., et al. 2020, [arXiv:1910.04121](#), *ApJS*, **247**, 25, The SPTpol Extended Cluster Survey
- Boselli, A., Fossati, M., & Sun, M. 2022, [arXiv:2109.13614](#), *A&A Rev.*, **30**, 3, Ram pressure stripping in high-density environments
- Brown, T., et al. 2017, [arXiv:1611.00896](#), *MNRAS*, **466**, 1275, Cold gas stripping in satellite galaxies: from pairs to clusters
- Bulbul, E., et al. 2024, [arXiv:2402.08452](#), *A&A*, **685**, A106, The SRG/eROSITA All-Sky Survey. The first catalog of galaxy clusters and groups in the Western Galactic Hemisphere
- Butcher, H. & Oemler, A., J. 1984, *ApJ*, **285**, 426, The evolution of galaxies in clusters. V. A study of populations since $Z = 0.5$.
- Cautun, M., van de Weygaert, R., Jones, B. J. T., & Frenk, C. S. 2014, [arXiv:1401.7866](#), *MNRAS*, **441**, 2923, Evolution of the cosmic web
- Cava, A., et al. 2009, [arXiv:0812.2022](#), *A&A*, **495**, 707, WINGS-SPE Spectroscopy in the Wide-field Nearby Galaxy-cluster Survey
- CCAT-prime Collaboration. 2023, [arXiv:2107.10364](#), *ApJS*, **264**, 7, CCAT-prime Collaboration: Science Goals and Forecasts with Prime-Cam on the Fred Young Submillimeter Telescope
- CHEX-MATE Collaboration. 2021, [arXiv:2010.11972](#), *A&A*, **650**, A104, The Cluster HERitage project with XMM-Newton: Mass Assembly and Thermodynamics at the Endpoint of structure formation. I. Programme overview
- Clerc, N., et al. 2020, [arXiv:2007.05484](#), *MNRAS*, **497**, 3976, SPIDERS: overview of the X-ray galaxy cluster follow-up and the final spectroscopic data release
- Courtois, H. M., Dupuy, A., Guinet, D., Baulieu, G., Ruppin, F., & Brenas, P. 2023, [arXiv:2211.16390](#), *A&A*, **670**, L15, Gravity in the local Universe: Density and velocity fields using CosmicFlows-4
- Damsted, S., et al. 2023, [arXiv:2307.08749](#), *A&A*, **676**, A127, CODEX: Role of velocity substructure in the scaling relations of galaxy clusters
- Damsted, S., et al. 2024, [arXiv:2403.17055](#), *arXiv e-prints*, [arXiv:2403.17055](#), AXES-SDSS: comparison of SDSS galaxy groups with all-sky X-ray extended sources
- de Gasperin, F., et al. 2022, [arXiv:2111.06940](#), *A&A*, **659**, A146, MeerKAT view of the diffuse radio sources in Abell 3667 and their interactions with the thermal plasma
- de Jong, R. S., et al. 2016, in Society of Photo-Optical Instrumentation Engineers (SPIE) Conference Series, Vol. 9908, Ground-based and Airborne Instrumentation for Astronomy VI, ed. C. J. Evans, L. Simard, & H. Takami, 99081O
- de Jong, R. S., et al. 2019, [arXiv:1903.02464](#), *The Messenger*, **175**, 3, 4MOST: Project overview and information for the First Call for Proposals
- de Jong, R. S., et al. 2022, in Society of Photo-Optical Instrumentation Engineers (SPIE) Conference Series, Vol. 12184, Ground-based and Airborne Instrumentation for Astronomy IX, ed. C. J. Evans, J. J. Bryant, & K. Motohara, 1218414
- de Vos, K., Merrifield, M. R., & Hatch, N. A. 2024, [arXiv:2406.02196](#), *MNRAS*, **531**, 4383, Local versus global environment: the suppression of star formation in the vicinity of galaxy clusters
- Dey, A., et al. 2019, [arXiv:1804.08657](#), *AJ*, **157**, 168, Overview of the DESI Legacy Imaging Surveys
- Diemer, B. 2018, [arXiv:1712.04512](#), *ApJS*, **239**, 35, COLOSSUS: A Python Toolkit for Cosmology, Large-scale Structure, and Dark Matter Halos
- Dietl, J., Pacaud, F., Reiprich, T. H., Veronica, A., Migkas, K., Spinelli, C., Dolag, K., & Seidel, B. 2024, [arXiv:2401.17281](#), *arXiv e-prints*, [arXiv:2401.17281](#), Discovery of a >13 Mpc long X-ray filament between two galaxy clusters beyond three times their virial radii
- Donnan, C. T., Tojeiro, R., & Kraljic, K. 2022, [arXiv:2201.08757](#), *Nature Astronomy*, **6**, 599, The role of the cosmic web in the scatter of the galaxy stellar mass-gas metallicity relation
- Dünner, R., Araya, P. A., Meza, A., & Reisenegger, A. 2006, [astro-ph/0603709](#), *MNRAS*, **366**, 803, The limits of bound structures in the accelerating Universe
- Dupuy, A. & Courtois, H. M. 2023, [arXiv:2305.02339](#), *A&A*, **678**, A176, Dynamic cosmography of the local Universe: Laniakea and five more watershed superclusters
- Ebeling, H., Stephenson, L. N., & Edge, A. C. 2014, [arXiv:1312.6135](#), *ApJ*, **781**, L40, Jellyfish: Evidence of Extreme Ram-pressure Stripping in Massive Galaxy Clusters
- Einasto, M., et al. 2018, [arXiv:1810.12122](#), *A&A*, **620**, A149, Supercluster A2142 and collapse in action: infalling and merging groups and galaxy transformations
- Fasano, G., et al. 2006, [astro-ph/0507247](#), *A&A*, **445**, 805, WINGS: a WIdE-field Nearby Galaxy-cluster Survey. I. Optical imaging
- Finoguenov, A., et al. 2019, [arXiv:1903.02471](#), *The Messenger*, **175**, 39, 4MOST Consortium Survey 5: eROSITA Galaxy Cluster Redshift Survey
- Fleener, M. C., Rose, J. A., Christiansen, W. A., Hunstead, R. W., Johnston-Hollitt, M., Drinkwater, M. J., & Saunders, W. 2005, [astro-ph/0505361](#), *AJ*, **130**, 957, Large-Scale Velocity Structures in the Horologium-Reticulum Supercluster
- Fleener, M. C., Rose, J. A., Christiansen, W. A., Johnston-Hollitt, M., Hunstead, R. W., Drinkwater, M. J., & Saunders, W. 2006, [astro-ph/0512169](#), *AJ*, **131**, 1280, Redshifts and Velocity Dispersions of Galaxy Clusters in the Horologium-Reticulum Supercluster
- Fujita, Y. 2004, [astro-ph/0311193](#), *PASJ*, **56**, 29, Pre-Processing of Galaxies before Entering a Cluster
- Gnedin, O. Y. 2003, [astro-ph/0302497](#), *ApJ*, **582**, 141, Tidal Effects in Clusters of Galaxies
- Gullieuszik, M., et al. 2015, [arXiv:1503.02628](#), *A&A*, **581**, A41, OmegaWINGS: OmegaCAM-VST observations of WINGS galaxy clusters
- Gunn, J. E. & Gott, J. Richard, I. 1972, *ApJ*, **176**, 1, On the Infall of Matter Into Clusters of Galaxies and Some Effects on Their Evolution
- Haines, C., et al. 2023, *The Messenger*, **190**, 31, CHANCES: A CHileAN Cluster galaxy Evolution Survey
- Haines, C. P., et al. 2013, [arXiv:1307.1135](#), *ApJ*, **775**, 126, LoCuSS: The Steady Decline and Slow Quenching of Star Formation in Cluster Galaxies over the Last Four Billion Years
- Haines, C. P., et al. 2015, [arXiv:1504.05604](#), *ApJ*, **806**, 101, LoCuSS: The Slow Quenching of Star Formation in Cluster Galaxies and the Need for Pre-processing
- Haines, C. P., et al. 2018, *MNRAS*, **481**, 1055, Shapley Supercluster Survey: mapping the filamentary network connecting the clusters
- Hasan, F., et al. 2023, [arXiv:2303.08088](#), *ApJ*, **950**, 114, The Evolving Effect of Cosmic Web Environment on Galaxy Quenching
- Herbonnet, R., et al. 2020, [arXiv:1912.04414](#), *MNRAS*, **497**, 4684, CCCP and MENeCS: (updated) weak-lensing masses for 100 galaxy clusters
- Hilton, M., et al. 2021, [arXiv:2009.11043](#), *ApJS*, **253**, 3, The Atacama Cosmology Telescope: A Catalog of >4000 Sunyaev-Zel'dovich Galaxy Clusters

- Hou, A., Parker, L. C., & Harris, W. E. 2014, [arXiv:1404.7504](#), *MNRAS*, **442**, 406, The pre-processing of subhaloes in SDSS groups and clusters
- Ishiyama, T., et al. 2021, [arXiv:2007.14720](#), *MNRAS*, **506**, 4210, The Uchuu simulations: Data Release I and dark matter halo concentrations
- Ivezić, Ž., et al. 2019, [arXiv:0805.2366](#), *ApJ*, **873**, 111, LSST: From Science Drivers to Reference Design and Anticipated Data Products
- Jaffé, Y. L., Smith, R., Candlish, G. N., Poggianti, B. M., Sheen, Y.-K., & Verheijen, M. A. W. 2015, [arXiv:1501.03819](#), *MNRAS*, **448**, 1715, BUDHIES II: a phase-space view of H I gas stripping and star formation quenching in cluster galaxies
- Jaffé, Y. L., et al. 2016, [arXiv:1604.07832](#), *MNRAS*, **461**, 1202, BUDHIES - III: the fate of H I and the quenching of galaxies in evolving environments
- Jin, S., et al. 2024, [arXiv:2212.03981](#), *MNRAS*, **530**, 2688, The wide-field, multiplexed, spectroscopic facility WEAVE: Survey design, overview, and simulated implementation
- Kesebonye, K. C., Hilton, M., Knowles, K., Cotton, W. D., Clarke, T. E., Loubser, S. I., Moodley, K., & Sikhosana, S. P. 2023, [arXiv:2211.03492](#), *MNRAS*, **518**, 3004, The MeerKAT Galaxy Clusters Legacy Survey: star formation in massive clusters at $0.15 < z < 0.35$
- Khalil, H., Finoguenov, A., Tempel, E., & Mamon, G. A. 2024, [arXiv:2403.17061](#), *arXiv e-prints*, [arXiv:2403.17061](#), AXES-2MRS: A new all-sky catalogue of extended X-ray galaxy groups
- Kluge, M., et al. 2024, [arXiv:2402.08453](#), *A&A*, **688**, A210, The SRG/eROSITA All-Sky Survey. Optical identification and properties of galaxy clusters and groups in the western galactic hemisphere
- Knuth, K. H. 2006, [physics/0605197](#), *arXiv e-prints*, [physics/0605197](#), Optimal Data-Based Binning for Histograms
- Kuchner, U., et al. 2022, [arXiv:2111.11467](#), *MNRAS*, **510**, 581, An inventory of galaxies in cosmic filaments feeding galaxy clusters: galaxy groups, back-splash galaxies, and pristine galaxies
- Kulier, A., et al. 2023, [arXiv:2305.03758](#), *ApJ*, **954**, 177, Ram Pressure Stripping in the EAGLE Simulation
- Lima, E. V. R., et al. 2022, [arXiv:2110.13901](#), *Astronomy and Computing*, **38**, 100510, Photometric redshifts for the S-PLUS Survey: Is machine learning up to the task?
- Lopes, P. A. A., Ribeiro, A. L. B., & Brambila, D. 2024, [arXiv:2309.11578](#), *MNRAS*, **527**, L19, The role of groups in galaxy evolution: compelling evidence of pre-processing out to the turnaround radius of clusters
- Lopez, S., et al. 2008, [arXiv:0803.0598](#), *ApJ*, **679**, 1144, Galaxy Clusters in the Line of Sight to Background Quasars. I. Survey Design and Incidence of Mg II Absorbers at Cluster Redshifts
- Lucey, J. R., Dickens, R. J., Mitchell, R. J., & Dawe, J. A. 1983, *MNRAS*, **203**, 545, The Horologium-Reticulum supercluster of galaxies.
- Lyke, B. W., et al. 2020, [arXiv:2007.09001](#), *ApJS*, **250**, 8, The Sloan Digital Sky Survey Quasar Catalog: Sixteenth Data Release
- Mamon, G. A., Sanchis, T., Salvador-Solé, E., & Solanes, J. M. 2004, [astro-ph/0310709](#), *A&A*, **414**, 445, The origin of H I-deficiency in galaxies on the outskirts of the Virgo cluster. I. How far can galaxies bounce out of clusters?
- Martínez, H. J., Muriel, H., & Coenda, V. 2016, [arXiv:1510.00390](#), *MNRAS*, **455**, 127, Galaxies infalling into groups: filaments versus isotropic infall
- McClintock, T., et al. 2019, [arXiv:1805.00039](#), *MNRAS*, **482**, 1352, Dark Energy Survey Year 1 results: weak lensing mass calibration of redMaPPer galaxy clusters
- McGee, S. L., Balogh, M. L., Bower, R. G., Font, A. S., & McCarthy, I. G. 2009, [arXiv:0908.0750](#), *MNRAS*, **400**, 937, The accretion of galaxies into groups and clusters
- Mendes de Oliveira, C., et al. 2019, [arXiv:1907.01567](#), *MNRAS*, **489**, 241, The Southern Photometric Local Universe Survey (S-PLUS): improved SEDs, morphologies, and redshifts with 12 optical filters
- Merloni, A., et al. 2019, [arXiv:1903.02472](#), *The Messenger*, **175**, 42, 4MOST Consortium Survey 6: Active Galactic Nuclei
- Merloni, A., et al. 2024, [arXiv:2401.17274](#), *A&A*, **682**, A34, The SRG/eROSITA all-sky survey. First X-ray catalogues and data release of the western Galactic hemisphere
- Merluzzi, P., et al. 2015, [arXiv:1407.4628](#), *MNRAS*, **446**, 803, Shapley Supercluster Survey: Galaxy evolution from filaments to cluster cores
- Miller, C. J., Stark, A., Gifford, D., & Kern, N. 2016, [arXiv:1612.05565](#), *ApJ*, **822**, 41, Inferring Gravitational Potentials from Mass Densities in Clusterized Halos
- Montaguth, G. P., et al. 2024, [arXiv:2406.14671](#), *arXiv e-prints*, [arXiv:2406.14671](#), Galaxy evolution in compact groups II. Witnessing the influence of major structures in their evolution
- Moretti, A., et al. 2014, [arXiv:1403.1408](#), *A&A*, **564**, A138, WINGS Data Release: a database of galaxies in nearby clusters
- Moretti, A., et al. 2017, [arXiv:1701.02590](#), *A&A*, **599**, A81, OmegaWINGS: spectroscopy in the outskirts of local clusters of galaxies
- Munari, E., Biviano, A., Borgani, S., Murante, G., & Fabjan, D. 2013, [arXiv:1301.1682](#), *MNRAS*, **430**, 2638, The relation between velocity dispersion and mass in simulated clusters of galaxies: dependence on the tracer and the baryonic physics
- Muzzin, A., et al. 2014, [arXiv:1402.7077](#), *ApJ*, **796**, 65, The Phase Space and Stellar Populations of Cluster Galaxies at $z \sim 1$: Simultaneous Constraints on the Location and Timescale of Satellite Quenching
- Natarajan, P., Kneib, J.-P., & Smail, I. 2002, [astro-ph/0207049](#), *ApJ*, **580**, L11, Evidence for Tidal Stripping of Dark Matter Halos in Massive Cluster Lenses
- Navarro, J. F., Frenk, C. S., & White, S. D. M. 1996, [astro-ph/9508025](#), *ApJ*, **462**, 563, The Structure of Cold Dark Matter Halos
- Okabe, N. & Smith, G. P. 2016, [arXiv:1507.04493](#), *MNRAS*, **461**, 3794, Lo-CuSS: weak-lensing mass calibration of galaxy clusters
- O’Kane, C. J., Kuchner, U., Gray, M. E., & Aragón-Salamanca, A. 2024, [arXiv:2409.09028](#), *MNRAS*, The effect of cosmic web filaments on galaxy evolution
- Oman, K. A., Hudson, M. J., & Behroozi, P. S. 2013, [arXiv:1301.6757](#), *MNRAS*, **431**, 2307, Disentangling satellite galaxy populations using orbit tracking in simulations
- Pallero, D., Gómez, F. A., Padilla, N. D., Bahé, Y. M., Vega-Martínez, C. A., & Torres-Flores, S. 2022, [arXiv:2012.08593](#), *MNRAS*, **511**, 3210, Too dense to go through: the role of low-mass clusters in the pre-processing of satellite galaxies
- Piffaretti, R., Arnaud, M., Pratt, G. W., Pointecouteau, E., & Melin, J. B. 2011, [arXiv:1007.1916](#), *A&A*, **534**, A109, The MCXC: a meta-catalogue of x-ray detected clusters of galaxies
- Piraino-Cerda, F., et al. 2024, [arXiv:2401.06973](#), *MNRAS*, **528**, 919, Pre- and post-processing of cluster galaxies out to $5 \times R_{200}$: the extreme case of A2670
- Pizzardo, M., Geller, M. J., Kenyon, S. J., & Damjanov, I. 2024, [arXiv:2311.10854](#), *A&A*, **683**, A82, The splashback radius and the radial velocity profile of galaxy clusters in IllustrisTNG
- Planck Collaboration. 2016, [arXiv:1502.01589](#), *A&A*, **594**, A13, Planck 2015 results. XIII. Cosmological parameters
- Planck Collaboration. 2020, [arXiv:1807.06209](#), *A&A*, **641**, A6, Planck 2018 results. VI. Cosmological parameters
- Proust, D., et al. 2006, [astro-ph/0509903](#), *A&A*, **447**, 133, Structure and dynamics of the Shapley Supercluster. Velocity catalogue, general morphology and mass
- Quilis, V., Planelles, S., & Ricciardelli, E. 2017, [arXiv:1703.09446](#), *MNRAS*, **469**, 80, Is ram-pressure stripping an efficient mechanism to remove gas in galaxies?
- Raj, M. A., et al. 2024, [arXiv:2407.03225](#), *arXiv e-prints*, [arXiv:2407.03225](#), The large-scale structure around the Fornax-Eridanus Complex
- Reiprich, T. H. & Böhringer, H. 2002, [astro-ph/0111285](#), *ApJ*, **567**, 716, The Mass Function of an X-Ray Flux-limited Sample of Galaxy Clusters
- Reiprich, T. H., et al. 2021, [arXiv:2012.08491](#), *A&A*, **647**, A2, The Abell 3391/95 galaxy cluster system. A 15 Mpc intergalactic medium emission filament, a warm gas bridge, infalling matter clumps, and (re-) accelerated plasma discovered by combining SRG/eROSITA data with ASKAP/EMU and DECAM data
- Reisenegger, A., Quintana, H., Carrasco, E. R., & Maze, J. 2000, [astro-ph/0007211](#), *AJ*, **120**, 523, The Shapley Supercluster. III. Collapse Dynamics and Mass of the Central Concentration
- Rines, K. & Diaferio, A. 2006, [astro-ph/0602032](#), *AJ*, **132**, 1275, CIRS: Cluster Infall Regions in the Sloan Digital Sky Survey. I. Infall Patterns and Mass Profiles
- Rosati, P., et al. 2014, *The Messenger*, **158**, 48, CLASH-VLT: A VIMOS Large Programme to Map the Dark Matter Mass Distribution in Galaxy Clusters and Probe Distant Lensed Galaxies
- Rykoff, E. S., et al. 2014, [arXiv:1303.3562](#), *ApJ*, **785**, 104, redMaPPer. I. Algorithm and SDSS DR8 Catalog
- Sereno, M. 2015, [arXiv:1409.5435](#), *MNRAS*, **450**, 3665, CoMaLit - III. Literature catalogues of weak lensing clusters of galaxies (LC^2)
- Sifón, C. & Han, J. 2024, [arXiv:2312.12529](#), *A&A*, **686**, A163, The history and mass content of cluster galaxies in the EAGLE simulation
- Simons Observatory Collaboration. 2019, [arXiv:1808.07445](#), *J. Cosmology Astropart. Phys.*, **2019**, 056, The Simons Observatory: science goals and forecasts
- Smith, R., Calderón-Castillo, P., Shin, J., Raouf, M., & Ko, J. 2022, [arXiv:2207.05099](#), *AJ*, **164**, 95, The First Fall is the Hardest: The Importance of Peculiar Galaxy Dynamics at Infall Time for Tidal Stripping Acting at the Centers of Groups and Clusters
- Smith, R., Choi, H., Lee, J., Rhee, J., Sanchez-Janssen, R., & Yi, S. K. 2016, [arXiv:1610.04264](#), *ApJ*, **833**, 109, The Preferential Tidal Stripping of Dark Matter versus Stars in Galaxies
- Stroe, A., Sobral, D., Paulino-Afonso, A., Alegre, L., Calhau, J., Santos, S., & van Weeren, R. 2017, [arXiv:1611.03512](#), *MNRAS*, **465**, 2916, A large $H\alpha$ survey of star formation in relaxed and merging galaxy cluster environments at $z \sim 0.15-0.3$
- Tempel, E., Kruuse, M., Kipper, R., Tuvikene, T., Sorce, J. G., & Stoica, R. S. 2018, [arXiv:1806.04469](#), *A&A*, **618**, A81, Bayesian group finder based on marked point processes. Method and feasibility study using the 2MRS data set

- Tempel, E., Tuvikene, T., Kipper, R., & Libeskind, N. I. 2017, [arXiv:1704.04477](#), *A&A*, **602**, A100, Merging groups and clusters of galaxies from the SDSS data. The catalogue of groups and potentially merging systems
- Tempel, E., et al. 2020a, [arXiv:2007.03307](#), *MNRAS*, **497**, 4626, An optimized tiling pattern for multiobject spectroscopic surveys: application to the 4MOST survey
- Tempel, E., et al. 2020b, [arXiv:2001.09348](#), *A&A*, **635**, A101, Probabilistic fibre-to-target assignment algorithm for multi-object spectroscopic surveys
- Tollet, É., Cattaneo, A., Mamon, G. A., Moutard, T., & van den Bosch, F. C. 2017, [arXiv:1707.06264](#), *MNRAS*, **471**, 4170, On stellar mass loss from galaxies in groups and clusters
- Treu, T., Ellis, R. S., Kneib, J.-P., Dressler, A., Smail, I., Czoske, O., Oemler, A., & Natarajan, P. 2003, [astro-ph/0303267](#), *ApJ*, **591**, 53, A Wide-Field Hubble Space Telescope Study of the Cluster Cl 0024+16 at $z = 0.4$. I. Morphological Distributions to 5 Mpc Radius
- Veronica, A., et al. 2024, [arXiv:2311.07488](#), *A&A*, **681**, A108, The eROSITA view of the Abell 3391/95 field. Cluster outskirts and filaments
- Wilman, D. J., Oemler, A., J., Mulchaey, J. S., McGee, S. L., Balogh, M. L., & Bower, R. G. 2009, [arXiv:0811.4425](#), *ApJ*, **692**, 298, Morphological Composition of $z \sim 0.4$ Groups: The Site of S0 Formation
- Zabludoff, A. I., Zaritsky, D., Lin, H., Tucker, D., Hashimoto, Y., Sheckman, S. A., Oemler, A., & Kirshner, R. P. 1996, [astro-ph/9512058](#), *ApJ*, **466**, 104, The Environment of “E+A” Galaxies
- ²⁵ School of Physics, Astronomy, University of Nottingham, Nottingham NG7 2RD, UK
- ²⁶ Universidad de Chile
- ²⁷ School of Physics and Astronomy, University of Birmingham, Birmingham, B15 2TT, UK
- ²⁸ INAF-Padova Astronomical Observatory, Vicolo dell’Osservatorio 5, I-35122 Padova, Italy
- ²⁹ ESO
- ³⁰ Tartu Observatory, University of Tartu, Observatooriumi 1, Tõravere 61602, Estonia
- ³¹ Estonian Academy of Sciences, Kohtu 6, 10130 Tallinn, Estonia

-
- ¹ Instituto de Física, Pontificia Universidad Católica de Valparaíso, Casilla 4059, Valparaíso, Chile
- ² Department of Physics, University of Helsinki, Gustaf Hällströmin katu 2, 00560 Helsinki, Finland
- ³ Instituto de Astronomía y Ciencias Planetarias (INCT), Universidad de Atacama, Copayapu 485, Copiapó, Chile
- ⁴ Departamento de Física, Universidad Técnica Federico Santa María, Avenida España 1680, Valparaíso, Chile
- ⁵ Institute of Astrophysics, Facultad de Ciencias Exactas, Universidad Andrés Bello, Sede Concepción, Talcahuano, Chile
- ⁶ Departamento de Astronomía, Instituto de Astronomía, Geofísica e Ciências Atmosféricas, Universidade de São Paulo, Rua do Matão 1226, Cidade Universitária, São Paulo, 05508-090, Brazil
- ⁷ Departamento de Astronomía, Universidad de La Serena, Avda. Raúl Bitrán 1305, La Serena, Chile
- ⁸ Instituto Multidisciplinario de Investigación y Postgrado, Raúl Bitrán 1305, La Serena, Chile
- ⁹ INAF - Osservatorio Astronomico di Capodimonte, Salita Moiarriello 16 80131 Napoli Italy
- ¹⁰ Centro Brasileiro de Pesquisas Físicas, Rua Dr. Xavier Sigaud 150, 22290-180 Rio de Janeiro, RJ, Brazil
- ¹¹ Departamento de Física Teórica y del Cosmos, Edificio Mecenas, Campus Fuentenueva, Universidad de Granada, E-18071, Granada, Spain
- ¹² Instituto Universitario Carlos I de Física Teórica y Computacional, Universidad de Granada, 18071 Granada, Spain
- ¹³ Instituto de Física y Astronomía, Universidad de Valparaíso, Avda. Gran Bretaña 1111, Valparaíso, Chile
- ¹⁴ Centre of Excellence for Data Science, Artificial Intelligence & Modelling, The University of Hull, Cottingham Road, Kingston-Upon-Hull, HU6 7RX, UK
- ¹⁵ Consejo Nacional de Investigaciones Científicas y Técnicas, Ciudad Autónoma de Buenos Aires, Argentina
- ¹⁶ Instituto de Astrofísica de La Plata, CONICET-UNLP, Paseo del Bosque s/n, B1900FWA, Argentina
- ¹⁷ Facultad de Ciencias Astronómicas y Geofísicas, Universidad Nacional de La Plata, Paseo del Bosque s/n, B1900FWA, Argentina
- ¹⁸ INAF-IASF Milano, Via Alfonso Corti 12, 20133, Milano, Italy
- ¹⁹ Max-Planck-Institut für extraterrestrische Physik (MPE), Gießenbachstraße 1, D-85748 Garching bei München
- ²⁰ Université Claude Bernard Lyon 1, IUF, IP2I Lyon, 4 rue Enrico Fermi, 69622 Villeurbanne, France
- ²¹ Institute of Astronomy, University of Cambridge, Madingley Road, Cambridge CB3 0HA, United Kingdom
- ²² Korea Institute for Advanced Study, 85, Hoegi-ro, Dongdaemun-gu, Seoul 02455, Republic of Korea
- ²³ Kuffner Observatory, Johann-Staud-Straße 10, 1160 Wien, Austria
- ²⁴ CASU, Institute of Astronomy, Cambridge, UK

Appendix A: CHANCES cluster samples

Tables A.1 and A.2 list the CHANCES cluster samples for the Low- z and Evolution subsurveys, respectively, along with the mass estimates and corresponding r_{200} . All of these clusters will be observed out to $5r_{200}$ with the 4MOST spectrograph through the five-year duration of the CHANCES survey.

Table A.1. CHANCES Low-z cluster sample. Clusters which are part of the Shapely and Horologium-Reticulum superclusters, which are also part of the Low-z survey, are not included in this table.

(1) Cluster name	(2) RA hh:mm:ss	(3) Dec dd:mm:ss	(4) Redshift	(5) M_{200} $10^{14} M_{\odot}$	(6) r_{200} Mpc	(7) θ_{200} arcmin	(8) Mass source
Abell 85	00:41:49.9	-09:18:07.2	0.056	8.4	1.96	29.00	MENeaCS
Abell 119	00:56:16.1	-01:15:18.0	0.044	7.8	1.92	35.63	MENeaCS
Abell 133	01:02:41.8	-21:52:55.2	0.057	4.1	1.54	22.45	MENeaCS
Abell 147	01:08:11.5	+02:10:33.6	0.044	1.4	1.08	20.10	MCXC
Abell 151	01:08:50.9	-15:24:25.2	0.053	2.5	1.30	20.28	MCXC
Abell 168	01:15:02.4	+00:18:54.0	0.044	2.4	1.29	24.04	MCXC
Abell 194	01:25:50.4	-01:24:07.2	0.017	0.6	0.83	38.79	AXES-2MRS
Abell 496	04:33:38.4	-13:15:32.4	0.034	5.7	1.73	41.61	AXES-2MRS
Abell 500	04:38:51.8	-22:06:00.0	0.067	3.0	1.37	17.26	MCXC
Abell 548	05:48:29.0	-25:28:58.8	0.041	2.7	1.34	26.63	MCXC
Abell 754	09:08:31.9	-09:36:57.6	0.054	14.9	2.37	36.33	MENeaCS
Abell 780	09:18:06.0	-12:04:58.8	0.057	6.5	1.80	26.20	MENeaCS
Abell 957	10:13:37.9	-00:54:57.6	0.045	2.2	1.25	22.83	MCXC
Abell 970	10:17:33.8	-10:39:57.6	0.059	3.6	1.48	20.85	MCXC
Abell 1069	10:39:43.0	-08:40:58.8	0.062	1.5	1.10	14.79	WINGS
Abell 1520	12:19:19.7	-13:15:36.0	0.068	3.7	1.48	18.29	MCXC
Abell 1631	12:52:51.8	-15:24:00.0	0.047	2.4	1.29	22.59	WINGS
Abell 1644	12:57:10.8	-17:24:00.0	0.048	6.0	1.76	30.11	WINGS
Abell 2399	21:57:22.1	-07:48:39.6	0.058	3.4	1.44	20.67	WINGS
Abell 2415	22:05:39.4	-05:35:38.4	0.058	1.5	1.11	15.87	WINGS
Abell 2457	22:35:40.8	+01:30:21.6	0.058	2.0	1.22	17.47	WINGS
Abell 2717	00:03:13.0	-35:55:58.8	0.050	1.4	1.09	17.93	WINGS
Abell 2734	00:11:20.6	-28:51:18.0	0.061	2.4	1.28	17.56	WINGS
Abell 2870	01:07:43.9	-46:54:00.0	0.023	4.5	1.59	55.14	CODEX
Abell 2877	01:10:00.2	-45:55:22.8	0.024	1.2	1.05	34.83	AXES-2MRS
Abell 3223	04:08:16.1	-30:53:38.4	0.060	3.0	1.38	19.25	MCXC
Abell 3266	04:31:13.0	-61:27:00.0	0.054	7.0	1.84	28.21	SPT-SZ
Abell 3301	05:00:46.6	-38:40:40.8	0.054	2.4	1.30	19.89	MCXC
Abell 3341	05:25:34.1	-31:35:42.0	0.037	1.9	1.20	25.96	AXES-2MRS
Abell 3376	06:00:40.8	-40:01:58.8	0.046	4.0	1.53	27.36	WINGS
Abell 3391	06:26:22.8	-53:41:49.2	0.051	4.3	1.56	25.32	MCXC
Abell 3395	06:27:36.0	-54:25:58.8	0.050	5.1	1.65	27.28	PSZ2
Abell 3490	11:45:19.9	-34:19:58.8	0.069	3.0	1.38	16.91	AXES-LEGACY
Abell 3497	12:00:03.8	-31:22:58.8	0.068	3.1	1.39	17.22	WINGS
Abell 3526	12:48:47.8	-41:18:28.8	0.011	2.8	1.37	98.26	AXES-2MRS
Abell 3565	13:36:39.1	-33:57:31.2	0.013	0.2	0.60	36.67	MCXC
Abell 3571	13:47:28.3	-32:50:56.4	0.039	8.7	1.99	41.49	AXES-2MRS
Abell 3574	13:49:06.7	-30:19:33.6	0.016	2.7	1.36	67.25	AXES-2MRS
Abell 3581	14:07:28.1	-27:00:54.0	0.023	2.0	1.23	42.74	AXES-2MRS
Abell 3651	19:52:16.3	-55:03:43.2	0.060	2.9	1.37	19.01	MCXC
Abell 3667	20:12:26.9	-56:48:57.6	0.053	8.2	1.94	30.28	ACT-DR5
Abell 3716	20:51:30.0	-52:42:57.6	0.045	4.5	1.60	29.12	WINGS
Abell 3809	21:46:58.8	-43:52:58.8	0.063	1.0	0.97	12.85	WINGS
Abell 4059	23:57:00.0	-34:45:32.4	0.048	6.2	1.77	30.28	ACT-DR5
Abell S560	06:00:48.2	-58:35:13.2	0.037	0.8	0.91	19.90	AXES-2MRS
Antlia	10:30:03.4	-35:19:22.8	0.009	1.3	1.06	92.08	PSZ2
Fornax	03:38:27.8	-35:26:52.8	0.005	0.3	0.69	107.25	MCXC
Hydra (A1060)	10:36:41.8	-27:31:26.4	0.012	2.2	1.26	82.82	AXES-2MRS
IIZw108	21:13:55.9	+02:33:54.0	0.048	1.5	1.11	19.09	WINGS
MKW4	12:04:27.6	+01:53:42.0	0.020	1.4	1.08	42.82	AXES-2MRS
MKW8	14:40:42.2	+03:28:19.2	0.027	1.4	1.09	32.46	AXES-2MRS

Notes. Columns are: (1) literature cluster name; (2) and (3): right ascension and declination corresponding to the adopted cluster centre; (5): literature cluster redshift; (6) and (7): mass and corresponding radius enclosing a mean density of 200 times the critical mass density of the Universe at the cluster redshift; (8) cluster angular size, $\theta_{200} = r_{200}/D_A$, where D_A is the angular diameter distance; (9) catalogue from which we take the cluster mass, after normalizing the published masses as discussed in [Section 3](#).

Table A.2. CHANCES Evolution sample.

Cluster name	RA hh:mm:ss	Dec dd:mm:ss	Redshift	M_{200} $10^{14} M_{\odot}$	r_{200} Mpc	θ_{200} arcmin	Mass source
Abell 209	01:31:53.5	-13:36:46.8	0.209	8.5	1.86	8.80	MENeaCS
Abell 370	02:39:50.4	-01:35:06.0	0.373	24.1	2.47	7.76	MENeaCS
Abell 520	04:54:06.5	+02:57:43.2	0.203	11.5	2.07	9.99	MENeaCS
Abell 521	04:54:09.1	-10:14:20.4	0.247	5.8	1.62	6.74	LoCuSS
Abell 1300	11:31:54.5	-19:55:40.8	0.306	12.5	2.04	7.29	SPT-ECS
Abell 1437	12:00:26.2	+03:20:52.8	0.134	3.9	1.48	10.03	CoMaLit
Abell 1650	12:58:42.0	-01:45:32.4	0.085	10.5	2.09	21.21	MENeaCS
Abell 1651	12:59:28.1	-04:12:03.6	0.085	8.3	1.93	19.60	MENeaCS
Abell 1689	13:11:30.0	-01:20:06.0	0.183	11.4	2.07	10.86	LoCuSS
Abell 1835	14:00:52.3	+02:52:40.8	0.252	10.5	1.96	8.06	LoCuSS
Abell 2163	16:15:49.2	-06:09:07.2	0.206	13.1	2.15	10.30	MENeaCS
Abell 2420	22:10:16.6	-12:10:37.2	0.085	8.4	1.94	19.58	MENeaCS
Abell 2744	00:14:18.7	-30:23:20.4	0.308	20.6	2.41	8.58	CoMaLit
Abell 2811	00:42:08.6	-28:32:09.6	0.108	6.2	1.74	14.22	CoMaLit
Abell 2813	00:43:27.8	-20:37:01.2	0.292	8.5	1.80	6.66	LoCuSS
Abell 3048	02:46:27.6	-20:32:06.0	0.310	8.2	1.77	6.27	ACT-DR5
Abell 3186	03:52:14.6	-74:00:28.8	0.127	10.2	2.03	14.44	PSZ2
Abell 3378	06:05:52.6	-35:18:32.4	0.139	8.8	1.93	12.70	PSZ2
Abell 3404	06:45:29.3	-54:13:08.4	0.164	16.0	2.33	13.34	ACT-DR5
Abell 3444	10:23:50.9	-27:15:32.4	0.254	11.5	2.02	8.25	SPT-ECS
Abell 3695	20:34:49.4	-35:49:30.0	0.089	7.5	1.87	18.10	CoMaLit
Abell 3822	21:54:06.7	-57:51:46.8	0.076	5.3	1.67	18.68	ACT-DR5
Abell 3827	22:01:52.6	-59:56:20.4	0.098	12.5	2.20	19.62	ACT-DR5
Abell 3911	22:46:17.0	-52:43:19.2	0.097	6.7	1.79	16.11	PSZ2
Abell 3921	22:49:49.4	-64:24:54.0	0.094	7.0	1.82	16.77	SPT-SZ
Abell S780	14:59:29.3	-18:11:13.2	0.236	12.3	2.08	8.98	PSZ2
Bullet	06:58:31.0	-55:56:49.2	0.296	14.3	2.14	7.83	CoMaLit
MACS J0329.7-0211	03:29:41.5	-02:11:45.6	0.450	8.6	1.70	4.78	CoMaLit
MACS J0416.1-2403	04:16:09.8	-24:03:57.6	0.397	10.7	1.87	5.65	CoMaLit
MACS J0553.4-3342	05:53:27.1	-33:42:54.0	0.430	21.4	2.34	6.75	ACT-DR5
MACS J1206.2-0847	12:06:12.2	-08:48:00.0	0.441	18.1	2.19	6.22	CoMaLit
PSZ2 G205.93-39.64	04:17:37.4	-11:53:45.6	0.443	30.6	2.61	7.38	CoMaLit
PSZ2 G208.60-26.00	05:10:47.8	-08:01:44.4	0.219	13.0	2.14	9.74	ACT-DR5
PSZ2 G241.11-28.68	05:42:57.1	-35:59:02.4	0.420	10.0	1.82	5.32	ACT-DR5
PSZ2 G241.76-30.88	05:32:56.0	-37:01:34.0	0.275	14.7	2.18	8.40	ACT-DR5
PSZ2 G259.98-63.43	02:32:18.7	-44:20:42.0	0.284	17.3	2.29	8.63	ACT-DR5
PSZ2 G262.27-35.38	05:16:36.7	-54:31:12.0	0.295	9.5	1.87	6.86	CoMaLit
PSZ2 G262.73-40.92	04:38:19.0	-54:19:04.8	0.421	15.0	2.07	6.05	ACT-DR5
PSZ2 G271.18-30.95	05:49:18.2	-62:04:58.8	0.376	16.4	2.18	6.80	SPT-SZ
PSZ2 G277.76-51.74	02:54:23.0	-58:57:50.4	0.438	11.2	1.87	5.33	ACT-DR5
PSZ2 G286.98+32.90	11:50:49.2	-28:04:37.2	0.390	31.0	2.67	8.17	CoMaLit
PSZ2 G348.90-67.37	23:25:13.0	-41:12:28.8	0.358	10.9	1.91	6.15	ACT-DR5
RXC J0528.9-3827	05:28:53.0	-39:28:15.5	0.284	12.8	2.07	7.81	ACT-DR5
RXC J1314.4-2515	13:14:28.1	-25:15:39.6	0.244	13.8	2.16	9.06	SPT-ECS
RXC J1347.5-1144	13:47:30.5	-11:45:10.8	0.452	16.1	2.10	5.88	MENeaCS
RXC J1514.9-1523	15:14:58.1	-15:23:09.6	0.223	13.8	2.18	9.81	PSZ2
RXC J2031.8-4037	20:31:51.6	-40:37:15.6	0.341	14.7	2.13	7.07	ACT-DR5
RXC J2211.7-0350	22:11:43.4	-03:49:44.4	0.397	19.4	2.28	6.89	CoMaLit
RXC J2248.7-4431	22:48:43.4	-44:31:44.4	0.347	18.7	2.30	7.55	CoMaLit
SMACS J0723.3-7327	07:23:21.4	-73:26:20.4	0.390	12.8	1.99	6.09	PSZ2

Notes. Columns are as in Table A.1.